

We are IntechOpen, the world's leading publisher of Open Access books Built by scientists, for scientists

6,900

Open access books available

185,000

International authors and editors

200M

Downloads

Our authors are among the

154

Countries delivered to

TOP 1%

most cited scientists

12.2%

Contributors from top 500 universities



WEB OF SCIENCE™

Selection of our books indexed in the Book Citation Index
in Web of Science™ Core Collection (BKCI)

Interested in publishing with us?
Contact book.department@intechopen.com

Numbers displayed above are based on latest data collected.
For more information visit www.intechopen.com



Surface-Confined Ruthenium Complexes Bearing Benzimidazole Derivatives: Toward Functional Devices

Masa-aki Haga

Abstract

Substitutionally inert ruthenium complexes bearing benzimidazole derivatives have unique electrochemical and photochemical properties. In particular, proton coupled electron transfer (PCET) in ruthenium–benzimidazole complexes leads to rich redox chemistry, which allows e.g. the tuning of redox potentials or switching by deprotonation. Using the background knowledge from acquired from their solution-state chemistry, Ru complexes immobilized on electrode surfaces have been developed and these offer new research directions toward functional molecular devices. The integration of surface-immobilized redox-active Ru complexes with multilayer assemblies via the layer-by-layer (LbL) metal coordination method on ITO electrodes provides new types of functionality. To control the molecular orientation of the complexes on the ITO surface, free-standing tetrapodal phosphonic acid anchor groups were incorporated into tridentate 2,6-bis(benzimidazole-2-yl) pyridine or benzene ligands. The use of the LbL layer growth method also enables “coordination programming” to fabricate multilayered films, as a variety of Ru complexes with different redox potentials and pK_a values are available for incorporation into homo- and heterolayer films. Based on this strategy, many functional devices, such as scalable redox capacitors for energy storage, photo-responsive memory devices, proton rocking-chair-type redox capacitors, and protonic memristor devices have been successfully fabricated. Further applications of anchored Ru complexes in photoredox catalysis and dye-sensitized solar cells may be possible. Therefore, surface-confined Ru complexes exhibit great potential to contribute to the development of advanced functional molecular devices.

Keywords: Ru benzimidazole complex, surface immobilization, layer-by-layer assembly, molecular devices, redox chemistry, proton-coupled electron transfer (PCET), heterolayer, multilayer film, memory, phosphonic acid, redox capacitor, protonic memristor

1. Introduction

Ruthenium is a precious metal that belongs to the platinum-group elements [1]. As ruthenium can adopt various oxidation numbers, its coordination complexes adopt a wide variety of oxidation states from -II to VIII [2]. When nitrogen-based donor ligands are coordinated to a central ruthenium atom, the resulting ruthenium

complexes generally prefer the +II and + III oxidation states, but occasionally also adopt the +IV and + V states. Arguably the most studied Ru complexes with nitrogen-based donor ligands are those that contain the hexaammineruthenium dication, $[\text{Ru}(\text{NH}_3)_6]^{2+}$, and the tris(2,2'-bipyridine)ruthenium(II) dication, $[\text{Ru}(\text{bpy})_3]^{2+}$ (bpy = 2,2'-bipyridine) [3–6]. $[\text{Ru}(\text{bpy})_3]^{2+}$ was first reported by Burstall [7] and is easily obtained from the reaction of $\text{RuCl}_3 \cdot n\text{H}_2\text{O}$ with an excess amount of bpy in aqueous ethanol. $[\text{Ru}(\text{bpy})_3]^{2+}$ exhibits a stable low-spin t_{2g}^6 electronic configuration as well as a reversible one-electron oxidation at +1.29 V (vs SCE) and successive one-electron reductions at –1.33 V, –1.52 V, –1.76 V, and –2.4 V vs. SCE; the oxidation is a Ru(II/III) metal-center-based process, while the reductions occur on the bpy ligands. $[\text{Ru}(\text{bpy})_3]^{2+}$ exhibits a metal-to-ligand charge transfer (MLCT) band at 452 nm and bright luminescence at 612 nm (lifetime: 600 ns) under MLCT excitation. This luminescence arises from the triplet MLCT photoexcited state, which allows this complex to serve as a photosensitizer for a wide scope of photoenergy conversion processes and as a photocatalyst for organic transformations [8]. Therefore, it is hardly surprising that during the past five decades, numerous studies on photoactive $[\text{Ru}(\text{bpy})_3]^{2+}$ complexes have been reported [3]. The tuning of their physical properties, such as their absorption/emission maxima or redox potential, via ligand modification has been achieved by introducing substituents on bpy or by replacing the bpy ligand with other *N*-heteroaromatic ligands. This tuning has led to a wide range of functional materials based on $[\text{Ru}(\text{bpy})_3]^{2+}$.

For example, replacing one of the bpy ligands in $[\text{Ru}(\text{bpy})_3]^{2+}$ with an *N*-heteroaromatic ligand comprising a benzimidazole and a pyridine group shifts the Ru(II/III) oxidation potential in negative direction because benzimidazole is a stronger σ -donor and weaker π -acceptor than pyridine [9]. Furthermore, the coordinated benzimidazole N–H imino group acts as a Brønsted acid, and the corresponding deprotonated benzimidazolate site can coordinate to another metal ion (**Figure 1**) [10]. Protonated or *N*-alkyl benzimidazolium ions can act as precursors for *N*-heterocyclic carbene (NHC) metal complexes [11, 12]. The representative pyridine-containing ligands 2,2'-bipyridine (bpy) and 2,2',2''-terpyridine (tpy) form chelate complexes with bidentate and tridentate coordination modes. When one or two pyridine groups are replaced with benzimidazole, the resulting bidentate- and tridentate-coordinating ligands are known as 2-(2-pyridyl)benzimidazole and 2,6-bis(benzimidazol-2-yl)pyridine, respectively (**Figure 2**) [13, 14].

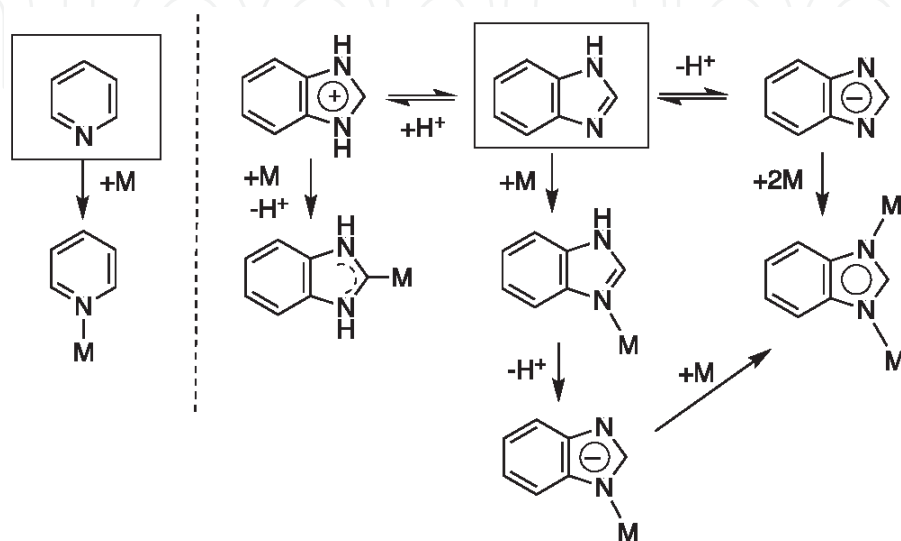


Figure 1.
Coordination modes of pyridine and benzimidazole as ligands.

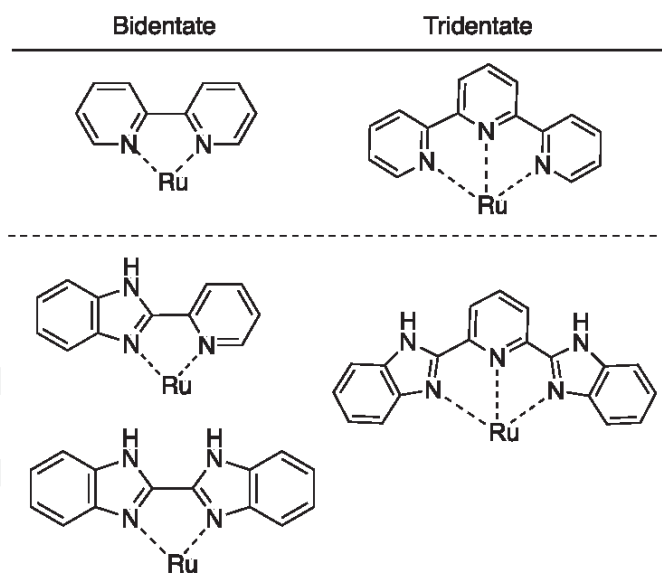


Figure 2.
Chemical structures of bidentate and tridentate ligands that contain pyridine and benzimidazole group(s).

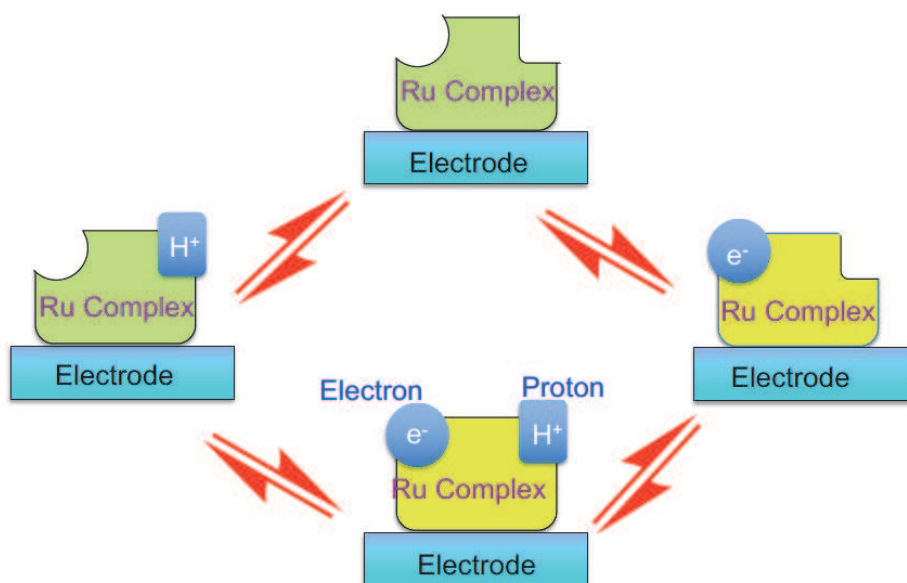


Figure 3.
Schematic illustration of molecular devices based on electron/proton-responsive Ru complexes confined to a surface.

This chapter focuses on the molecular design of ruthenium complexes with *N*-heteroaromatic ligands, particularly benzimidazole derivatives. In Ru–benzimidazole complexes in aqueous solution, the solution pH strongly affects the Ru(II/III) oxidation potential, which is derived from the proton-coupled electron transfer (PCET) reaction in solution [15]. The proton-responsiveness of Ru–benzimidazole complexes has been exploited to obtain switching functionality in multinuclear Ru complexes [16, 17]. In addition, ligand modification via *N*-alkylation of the benzimidazole N–H imino group has been used to achieve the anchoring of redox-active Ru complexes [18, 19]. and the layer-by-layer (LbL) assembly of Ru complexes on indium-tin oxide (ITO) surfaces toward molecular electronic devices [20–22].

Figure 3 presents a schematic illustration of our conceptual approach for molecular devices based on surface-confined Ru complexes with electron/proton-responsiveness.

2. Molecular design of functional Ru complexes with benzimidazole ligands

2.1 Bridging ligands that contain benzimidazole groups

Benzimidazole ligands can be synthesized by the Phillips condensation reaction between an organic carboxylic acid or nitrile and *o*-phenylenediamine [23].

Figure 4 shows the structures of benzimidazole ligands bridging two Ru centers that have been used by our group [17, 24–26] and others [27, 28] for the preparation of dinuclear Ru complexes. Depending on the chemical structure of the linker moiety, significant electronic coupling between the two ruthenium ions is possible. In addition, the oxidation processes of the Ru centers in aqueous solution involve PCET reactions, resulting in switching of the metal–metal interaction via the change in electron density on the conjugated linker ligand.

2.2 Introducing anchor groups in benzimidazole ligands

Surface modification plays an important role in controlling the electron-transfer events and chemical reactivity in photocatalysis, as well as the charge-transport process in heterojunctions. Recently, several reviews of the applications of surface modification toward dye-sensitized solar cells and electrochemical catalysts for hydrogen/oxygen-evolution reactions have been published [21, 29–34], showing the importance of such interdisciplinary research. In the area of solar-energy conversion, Grätzel-type dye-sensitized solar cells composed of mesoporous TiO₂ on fluorine-doped SnO₂ (FTO) with immobilized Ru complexes that contain 2,2'-bipyridyl-4,4'-dicarboxylate and other bpy-derived ligands have been developed [35]. Interestingly,

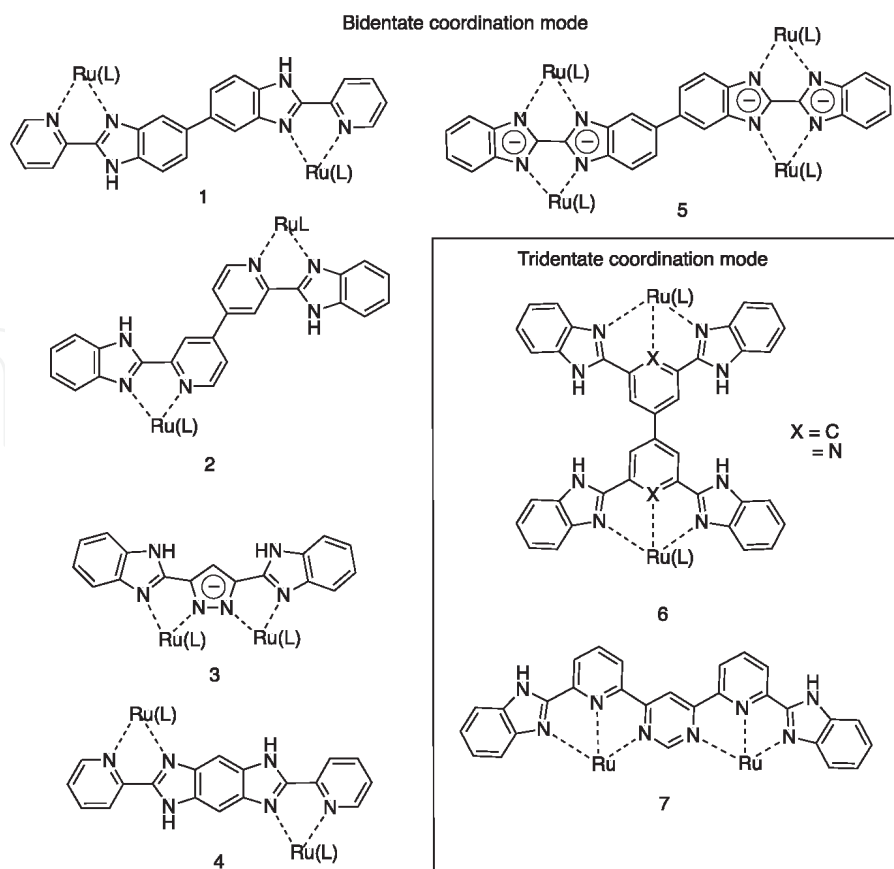


Figure 4. Chemical structures of benzimidazole-containing ligands that bridge two Ru centers in bis-bidentate or bis-tridentate coordination modes.

the electron-injection efficiency from the photoexcited-state Ru complex to TiO₂ was found to strongly dependent on the anchoring group [34, 36, 37].

Given that the adsorption strength of a Ru complex on a surface depends on the combination of the anchoring group and the surface material, judicious selection of both is necessary for effective surface functionalization. Recently, indium-tin oxide (ITO)-coated glass or polymer substrates have been employed in a wide variety of electronic display devices such as organic light-emitting diodes (OLEDs) [38]. Transparent ITO electrodes are also employed as cell windows for spectroelectrochemistry. Therefore, ITO is a suitable substrate for monitoring both the electrochemical and spectrochemical changes in redox-active Ru complexes immobilized on its surface. The phosphonic acid group, which is known to immobilize on ITO electrodes, has been employed to anchor the Ru complexes [39]. Furthermore, organic phosphonic acids are known to bind zirconium(IV) ions to form a solid two-dimensional layer structure, [40]. which demonstrates their suitability for use in a layer-by-layer growth method based on redox-active metal complexes. Therefore, we developed several new tridentate benzimidazole ligands with phosphonic acid or phosphonate ester anchor groups (**Figure 5**). Alkylation of the imino N–H groups of the benzimidazole moieties using bromoalkyl-diethylphosphonate derivatives furnished chelating benzimidazolyl ligands with ethyl-protected phosphonates, which were used for the synthesis of Ru complexes [41]. After the ethyl-protected phosphonate Ru complexes had been purified, the diethyl phosphonate groups were deprotected to provide the corresponding Ru complexes with phosphonic acid groups. In particular, the tridentate ligand **XP** (**Figure 5**) contains several methylene groups on its side-arms; these methylene moieties are sterically hindered, thus fixing the conformation of the phosphonic acid anchor groups upon surface immobilization.

2.3 Molecular design of redox-active Ru complexes with anchor groups

Ru complexes are substitutionally inert, and the octahedral coordination geometry around the Ru ion is maintained throughout the Ru(II/III) redox reaction. Therefore, they can be immobilized on a surface to design redox-active molecular devices. When three bidentate ligands are coordinated to an octahedral Ru complex, the formation of Δ and Λ optical isomers is possible, but in the case of Ru complexes surrounded by two tridentate ligands with C_{2v} symmetry, no optical isomers do not exist. Hence, surface-confined Ru complexes that contain tridentate ligands with C_{2v} symmetry such as 2,6-bis(benzimidazolyl)pyridine with phosphonic acid anchors are often selected for surface immobilization [21, 42]. Furthermore, the molecular orientation of Ru complexes self-assembled on a surface is crucial to the construction of further

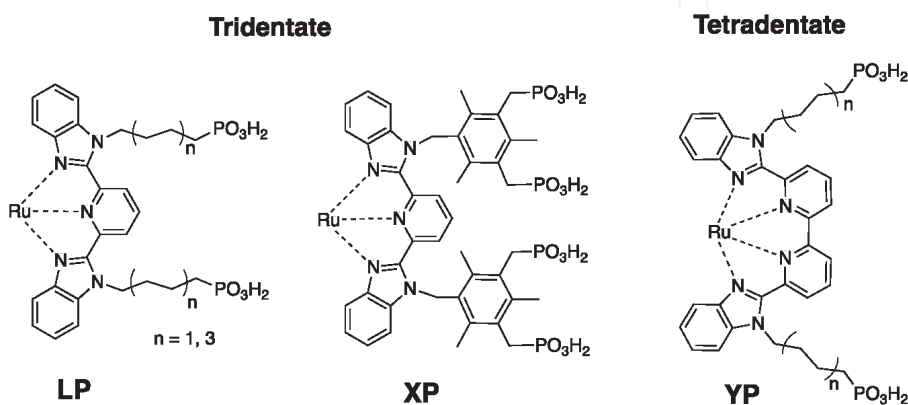


Figure 5.
 Chemical structures of benzimidazole-containing ligands with phosphonic acid anchor groups and their abbreviations.

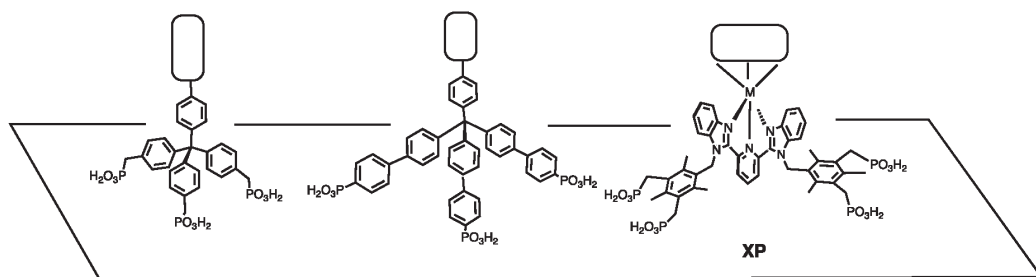


Figure 6. Chemical structures of free-standing multipodal phosphonic acid anchor groups on a surface [43–45].

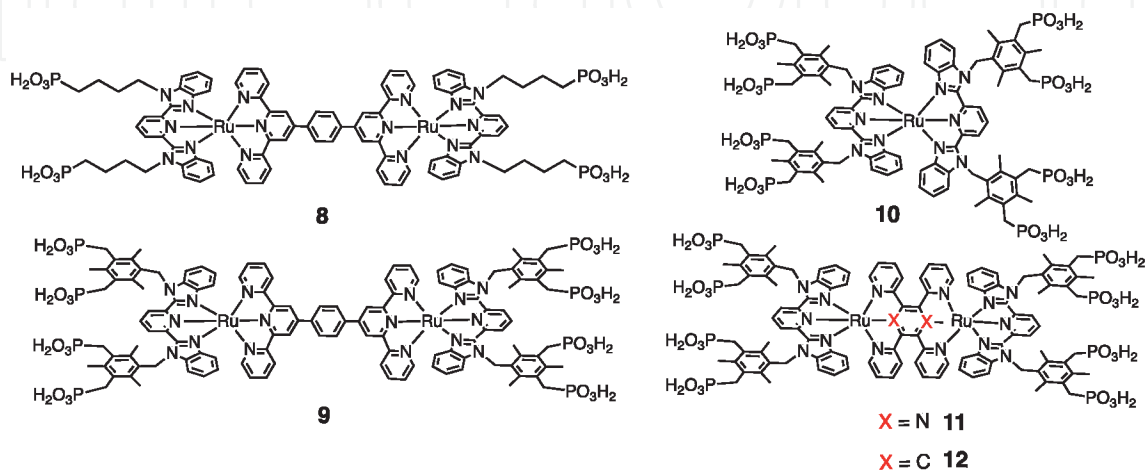


Figure 7. Chemical structures of rod-shaped dinuclear Ru complexes that bear free-standing multipodal anchor groups at both ends.

layered structures. To maintain the vertical orientation of the Ru complexes on a surface, free-standing multipodal anchor groups with phosphonic acid have been developed over the last two decades. Several examples are shown in **Figure 6** [21, 43–46], together with our multipodal tridentate benzimidazole ligand with phosphonate anchors, **XP**. **Figure 7** shows a new series of rod-shaped Ru complexes with 2,6-bis(benzimidazolyl)pyridine moieties and bi- or tetrapodal phosphonic acid groups at both ends that have been reported by our group. Mononuclear Ru complex **10** exhibits a spherical-shaped structure around the central Ru ion, while the other dinuclear Ru complexes **8**, **9**, **11**, and **12** exhibit a rod-like structure with a Ru–Ru axis [21, 43]. When the dinuclear Ru complexes are immobilized on a surface, the Ru–Ru axis can be oriented vertically or horizontally relative to the surface plane. In AFM measurements, the obtained molecular heights of the dinuclear Ru complexes **9**, **10**, and **11** immobilized on an ITO surface were consistent with the predicted heights for the vertical orientation of the dinuclear Ru complexes at the ITO surface. Ru complexes **8–12** can be dissolved in aqueous solution by adjusting the solution pH, given that the phosphonic acid groups at both ends of these act as polybasic acids.

3. Characterization and functionality of surface-immobilized redox-active Ru complexes

3.1 Surface modification by Ru complexes bearing phosphonic acid anchors

When Ru complexes bearing phosphonic acid anchors are immobilized on an ITO or mica surface by immersion of the substrate into a solution of the Ru

complex, the surface coverage of the Ru complex is dependent on the immersion time and the concentration of the complex in the solution. The temporal evolution of the surface coverage can be analyzed using the kinetic Langmuir equation (Eq. (1)), and curve fitting with a rate constant parameter, k .

$$\Gamma_t = \Gamma_s(1 - \exp(-kC^*t)) \quad (1)$$

Here, $\Gamma(t)$, k , C , and t refer to the surface coverage, rate constant, concentration of the Ru complex, and time, respectively [33, 46]. A typical kinetic plot for a Ru-XP complex with an acridine group at the top is shown in **Figure 8**. This surface-immobilized Ru-XP complex is able to capture double-stranded DNA from solution [46].

Another chemical approach to evaluate the surface coverage is using the thermodynamic Langmuir isotherm based upon the concentration dependence of the adsorption of the Ru complex.

$$\Gamma_i/(\Gamma_s - \Gamma_i) = \exp(\Delta G_{ads}^0/RT)C_B \quad (2)$$

Here, Γ_i , Γ_s , C_B , and ΔG_{ads} refer to the surface adsorption at a given concentration, the adsorption at saturation, the concentration of the bulk solution, and the free energy of adsorption, respectively. The adsorption of a Ru complex on a mica and ITO surface can be fitted with the typical Langmuir isotherm model. The free energy of adsorption for Ru complex **9** was found to be -33.4 kJ/mol.

In recent years, several binding modes for the absorption of phosphonic acid groups on metal oxides have been proposed based on intensive studies using polarization modulation infrared reflection adsorption spectroscopy (PM-IRRAS), X-ray photoelectron spectroscopy (XPS), and density functional theory (DFT) calculations in recent years, and the bidentate or tridentate binding modes are considered to be most probable (**Figure 9**) [30, 32, 34, 44, 47]. The optimum solution pH value for the adsorption of Ru complexes **8–12** depends on the complex; *i.e.*, pH = 6 is optimal for complexes **8–11**, while pH = 4 is better for complex **12**.

Atomic force microscopy (AFM) measurements have been used to provide clear surface images depicting the adsorption of these Ru complexes, particularly the surface morphology (*e.g.* height and surface coverage). **Figure 10** shows AFM images of Ru complex **9** on a flattened ITO surface. The samples were prepared using two different immersion conditions, *i.e.*, a dilute solution of the Ru complex with a short immersion time (1 μ M; 10 min) and a higher concentration solution with a longer immersion time (25 μ M; 3 h). As shown on the left in **Figure 10**, for the dilute

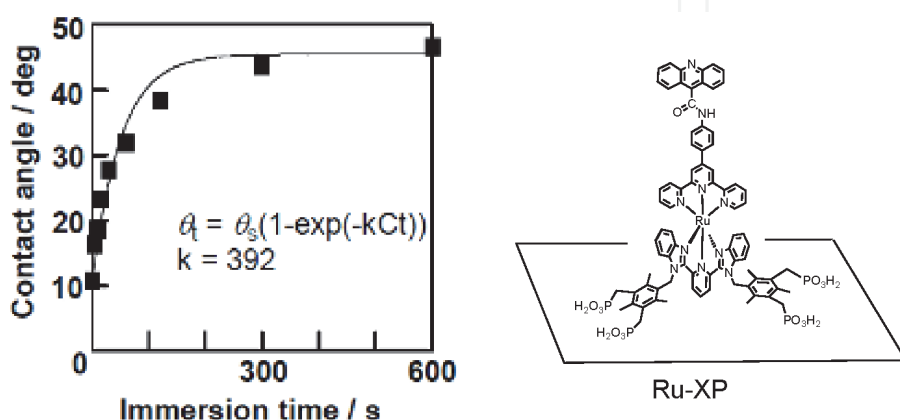


Figure 8.
Chemisorption kinetics of the Ru-XP complex determined by the temporal evolution of the surface coverage of the Ru-XP complex (right) on a mica surface. (left) Plot of contact angle versus immersion time [46].

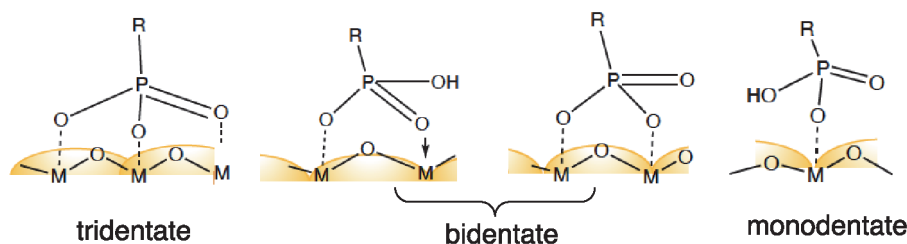


Figure 9. Proposed surface binding modes of phosphonic acid groups on a metal oxide (MO_x) surface ($M = \text{metal}$) [30].

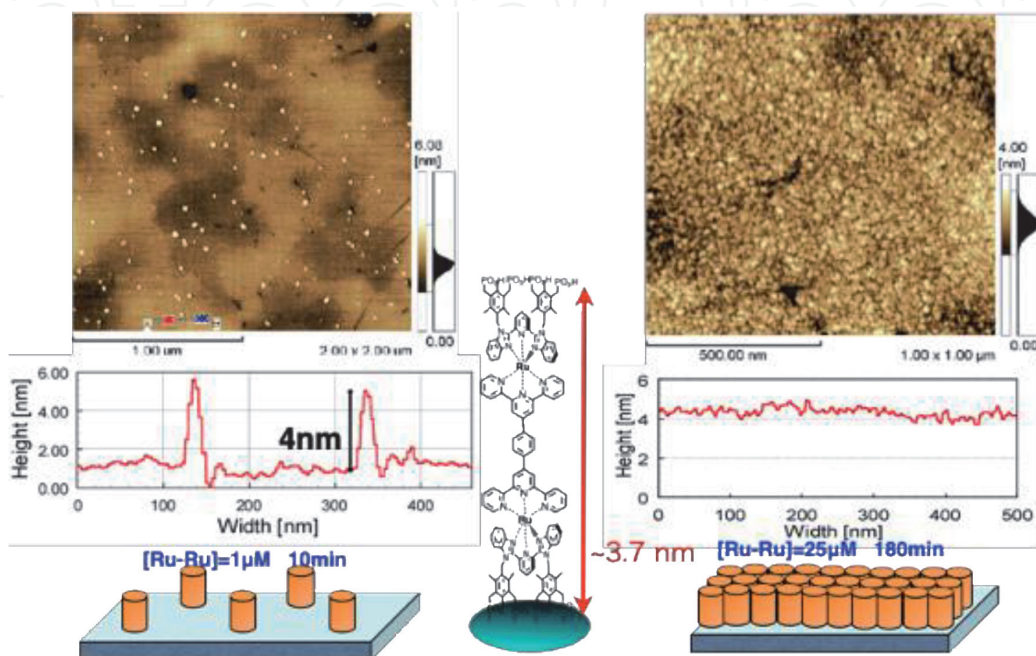


Figure 10. AFM images of dinuclear Ru complex **9** immobilized on a flat ITO surface using either a $1 \mu\text{M}$ solution of complex **9** with an immersion time of 10 min (left) or a $25 \mu\text{M}$ solution for 3 h (right). Plots show cross-sectional height profiles. In the schematic drawings of the surface images, **9** is shown as a cylinders.

condition, scattered dots were observed on the surface. The average height of the dots was approximately $4 \mu\text{m}$, which is consistent with the height that was predicted for vertically oriented complex **9** using a molecular model. The AFM image on the right in **Figure 10** shows that the surface was fully covered with spherical domains with a diameter of $\sim 20\text{--}50 \mu\text{m}$ when the concentrated conditions were used.

One advantage of ITO electrodes is that they enable the use of UV-vis spectroscopy to monitor the surface immobilization process. Ru(II) complexes bearing *N*-heteroaromatic ligands exhibit a relatively strong metal-to-ligand charge transfer (MLCT) band in the visible wavelength region. In particular, the temporal changes during the immobilization or multilayering processes of such complexes on modified ITO substrates are easily monitored via the absorbance changes in the UV-vis spectra. Furthermore, electrochemical methods such as cyclic voltammetry (CV) can be used to determine the surface coverage of redox-active Ru complexes immobilized on an ITO electrode [48].

3.2 PCET reaction of Ru-benzimidazole complexes in solution and on ITO electrodes

Ru complexes with benzimidazole derivative ligands act as Brønsted acids and exhibit proton-coupled electron transfer (PCET) reactions in aqueous solution [49, 50].

For example, $[\text{Ru}(\text{mbibzim})(\text{bibzimH}_2)]^{2+}$ (**13**) (mbibzim = 2,6-bis(1-methylbenzimidazol-2-yl)pyridine and bibzimH₂ = 2,6-bis(benzimidazole-2-yl)pyridine) behaves as a dibasic acid, as shown in **Figure 11**. The Ru(II/III) oxidation potential of **13**, which results from a PCET reaction, strongly depends on the pH-value ($2 < \text{pH} < 9$) in a Britton–Robinson buffer/CH₃CN(1:1 v/v) solution [14, 49, 50]. The PCET reaction of **13** can be described by the square scheme in **Figure 12**, in which complex **13** is abbreviated as Ru–LH₂. This reaction involves both electron transfer and proton-transfer equilibria. In the half-wave potential/pH plot of **13**, the so-called Pourbaix diagram, the half-wave potential is gradually shifted in the negative potential direction with increasing solution pH (**Figure 13**). Based on this diagram, the $\text{p}K_a$ values of **13** were determined to be 6.31 and 7.94 for the Ru(II) oxidation state, and < 2 and 3.60 for the Ru(III) oxidation state. When the central pyridine group in the bibzimH₂ ligand is replaced with a cyclometallated phenylene group, the resulting Ru complex **14** shows a lower Ru(II/III) oxidation potential than complex **13**; the $\text{p}K_a$ values of **14** also increase compared to those of **13**, *i.e.*, to 10.91 and > 12 for the Ru(II) oxidation state and to 6.46 and 9.15 for the Ru(III) oxidation state [51].

In biological systems, protons play a very important role in reactions and energy storage. Proton gradients are the driving force for the synthesis of ATP in biological membranes. Applications of proton gradients in energy storage in materials chemistry have shown that PCET chemical systems can be used for energy storage in redox batteries and capacitors. Ru complexes **13** and **14**, which show PCET with different potentials and $\text{p}K_a$ values in unbuffered aqueous solutions, have been used to construct two half-cells separated by a Nafion membrane [51]. The Pourbaix diagrams of complexes **13** and **14** are shown in **Figure 14**; the initial oxidation states of **13** and **14** were Ru(II) and Ru(III), respectively. Upon charging, the oxidation of **13** from the Ru(II) to the Ru(III) state releases the proton(s), while the reduction of **14** from Ru(III) to Ru(II) at the other half-cell captures the proton(s). As a result,

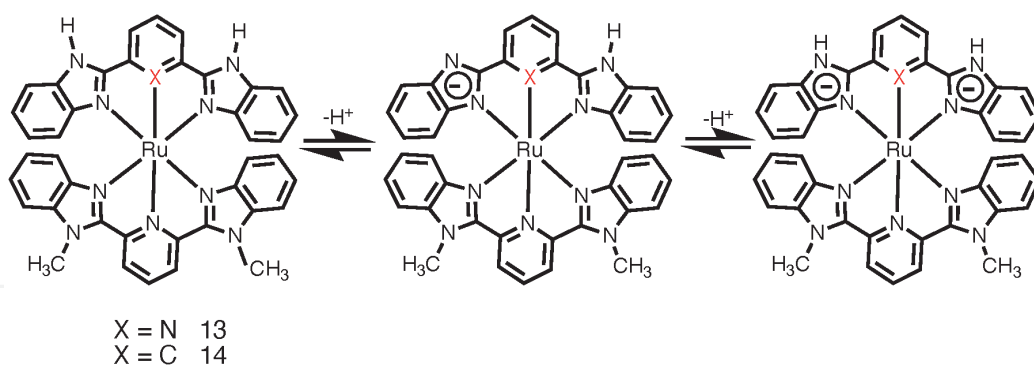


Figure 11. Stepwise proton-transfer equilibria of Ru(II)(LMe)(LH₂) complexes (**13**: X = N; **14**: X = C) that act as Brønsted dibasic acids. The total charge of the Ru complex is omitted.

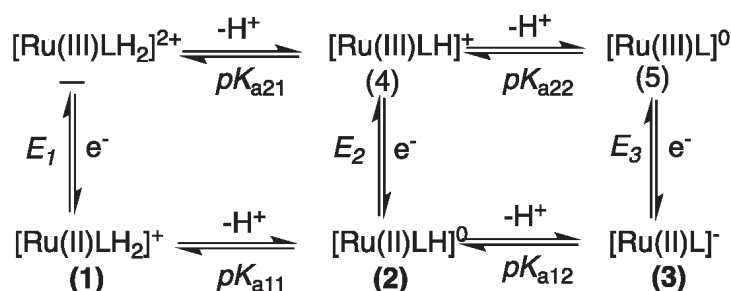


Figure 12. Square scheme of the electron–proton equilibria of Ru complexes **13** or **14** as dibasic acids. Numbers in parentheses indicate the Ru species present in the Pourbaix diagram in **Figure 13**.

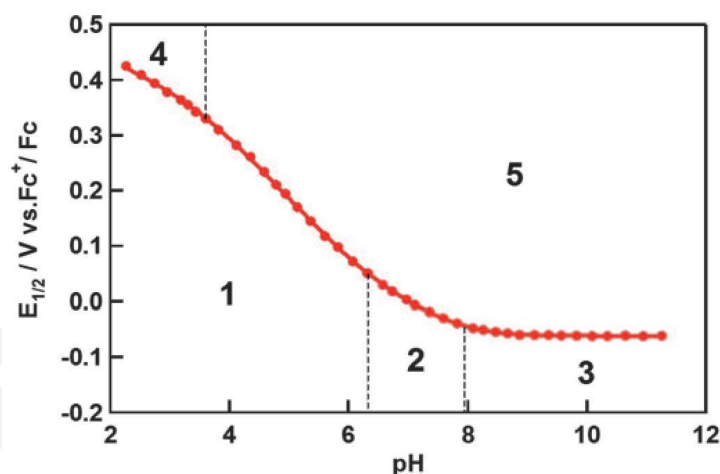


Figure 13.

Pourbaix diagram of Ru complex **13** in $\text{CH}_3\text{CN}/\text{BR}$ buffer (1/1 v/v) [51].

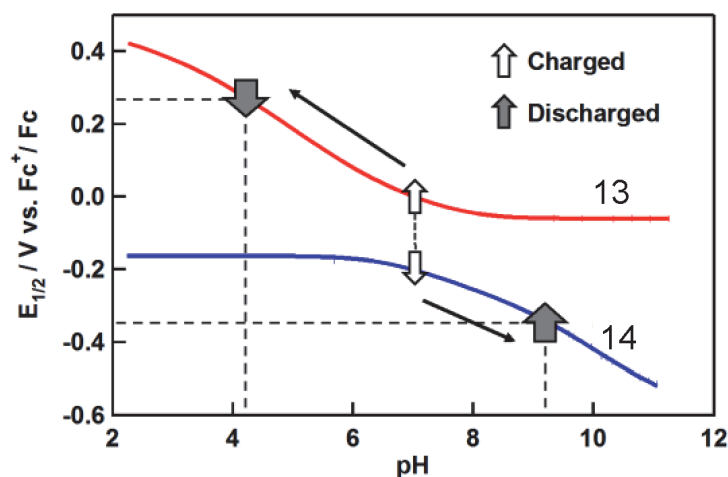


Figure 14.

Pourbaix diagram for a solution redox battery based on a pair of Ru complexes, **13** and **14**, which both exhibit PCET reactions in $\text{CH}_3\text{CN}/\text{BR}$ buffer (1/1 v/v).

the electrical energy was stored as a pH gradient between the half-cells. The concept of using a PCET system in this way had been implemented with organic quinone derivatives, [52] but its scope was extended to redox-flow batteries by using a pH-tunable Fe(III) azamacrocyclic complex as both the catholyte and anolyte based on the multiple protonated forms of the Fe complex [53].

The PCET chemistry of Ru complexes that contain benzimidazole derivatives in solution can be extended to surface-bound systems by attaching surface-anchoring groups to the Ru complexes as described in the previous section.

Dinuclear Ru complexes **15**, **16**, and **17** (Figure 15) have N–H sites that can be deprotonated on the bridging ligand and the phosphonic acid anchoring groups at both ends. When **15** and **16** are assembled on an ITO electrode, the surface-immobilized redox-active Ru(II) complexes exhibit a well-defined CV response with a typical shape derived from adsorbed chemical species [20]. Figure 16 shows the CV responses that originate from the Ru(II/III) oxidation process of immobilized complex **15** at different pH values; these responses arise from a well-defined two-electron oxidation wave corresponding to the Ru(II)–Ru(II)/Ru(III)–Ru(III) PCET process in **15** [24]. Upon changing the pH of the aqueous solution was changed, Ru complexes **8**–**17** immobilize stably via the phosphonic acid groups on the ITO electrode at pH = 1.0–9.0, but at pH > 9.5, the Ru complexes easily detached from the ITO surface.

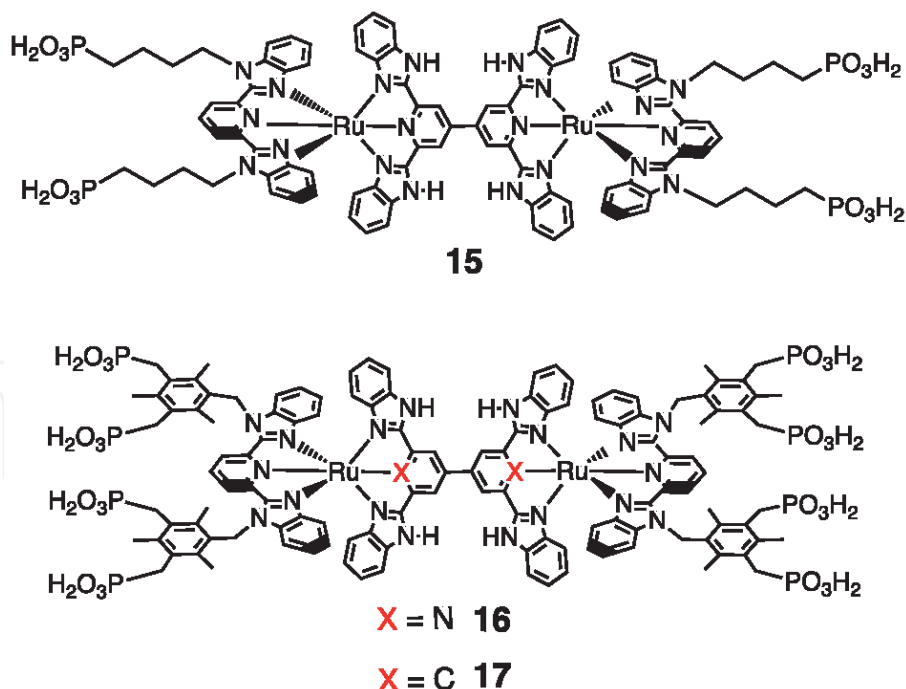


Figure 15.
Chemical structures of dinuclear Ru complexes bearing both a benzimidazole bridging ligand from which protons can dissociate and free-standing multipodal phosphonic acid anchor groups at both ends [24].

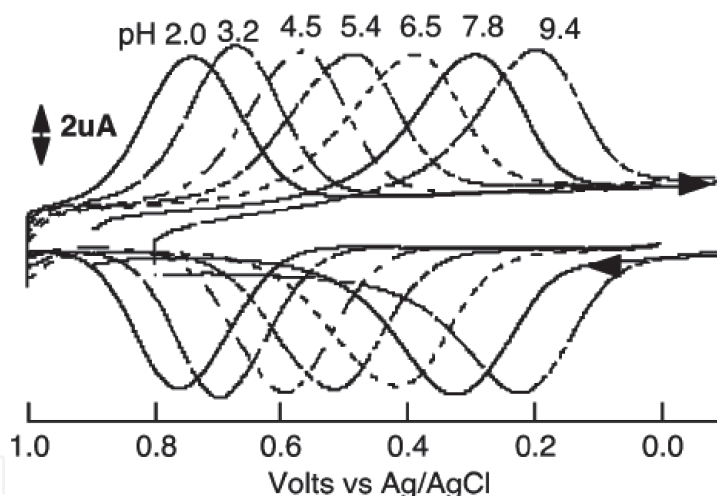


Figure 16.
Cyclic voltammograms of Ru complex **15** immobilized on an ITO electrode at different pH values in CH_3CN -BR buffer (1/1 v/v) [24].

The anodic peak current, i_{pa} , is expressed as shown in Eq. (3), where n , ν , A , and Γ represent the number of electrons, scan rate, electrode area, and surface coverage, respectively. Therefore, the anodic peak current for complex **15** is linearly proportional to the scan rate ν , indicating that the Ru complex is a surface-bound species. The total area of the anodic wave is related to the surface coverage of the Ru complex, which was determined to be $0.80 \times 10^{-10} \text{ mol cm}^{-2}$.

$$i_{pa} = \frac{n^2 F^2 \nu}{4RT} A \Gamma \quad (3)$$

Given that the spectral change due to the redox reactions of a monolayer film of **15** on the ITO electrode can be observed by UV-vis spectroscopy, even surface-assembled monolayer films of Ru complexes on an ITO electrode can be detected.

Upon the oxidation of **15** under an applied potential of +0.8 V vs. Ag–AgCl at pH = 6.5, the differential absorption spectrum demonstrates strong bleaching of the MLCT band at 550 nm and π - π^* transitions of the ligands at 364 nm, along with absorbance increases at 400 and \sim 750 nm, which are characteristic spectral features of Ru(III)–L complexes [24].

3.3 Fabrication of multilayer films based on Ru complexes by layer-by-layer (LbL) growth

Surface modification using a molecular monolayer film alone enables only a single set of functionalities to be incorporated, and the measurable physical quantities, such as optical absorption or current value, are very low due to the low molecular density on the surface. On the other hand, multi-layer modification has the advantages of allowing various molecular units to be deposited at the surface, achieving greater increases in physical quantities such as optical density and charge stored, and enables the integration of various functionalities at the interface [31]. Thus, the integration of functional metal complexes on an electrode holds great promise for applications in *e.g.* molecular-based devices for photochemical energy production/transduction, photocatalysis, and information storage, among other applications [54]. To achieve this integration, the LbL assembly method, in which multilayer structures are constructed via molecular interactions between two layers on a solid surface, is an appropriate technique [39]. LbL assembly using electrostatic interactions, [55]. hydrogen bonding, and coordination metal–ligand bonds has been reported [21, 56]. Among these, structures based on metal-coordination assembly are robust toward environmental changes, such as variations in pH or ionic strength, in aqueous solution.

The formation of well-ordered zirconium(IV) bisphosphonate multilayer films is a well-known method for LbL assemblies on a solid surface that has been developed by Mallouk and others [40]. This method is based on the reconstitution of a two-dimensional layered compound, $\text{Zr}(\text{HPO}_3)_2$, on a gold surface via self-assembly of molecular units with metal ions. Starting from self-assembled 4-mercaptobutylphosphonic acid on the gold surface as a primer layer, alternate immersion of the modified gold substrate into a zirconium(IV) oxychloride solution and a bisphosphonic acid solution leads to multilayer films composed of a two-dimensional zirconium–phosphonate framework structure via LbL growth [40].

Similarly, the rod-shaped Ru complexes **8–16** with polyphosphonic acid groups at both ends were immobilized by self-assembly on an ITO electrode. The polyphosphonic acids at one side of the complexes were attached to the ITO surface, while the other side of the polyphosphonic acid groups remained free to interact with metal ions in solution. Multilayer films of the Ru complexes could thus be obtained by successive alternate immersion in a zirconium(IV) ion and a Ru complex solution (**Figure 17**) [57]. The immobilized Ru film on the ITO substrate was monitored via UV–vis spectroscopy, CV, and the AFM-surface-scratching method throughout each stage of the LbL growth. The use of these monitoring techniques during LbL growth is shown in **Figure 18** with the combination of Ru complex **11** and zirconium as an example.

In each physical measurement, the physical quantities, such as absorbance, amount of charge, and the height of the scratch increased linearly with increasing number of layers. Two types of growth models have been proposed for LbL growth from the surface-primer points via metal coordination on a solid surface (**Figure 19**) [59]. The first model involves dendritic divergent growth, which would result in an exponential increase in the physical quantities, while the second model involves linear growth of a layered structure. In the case of Ru complex **11**,

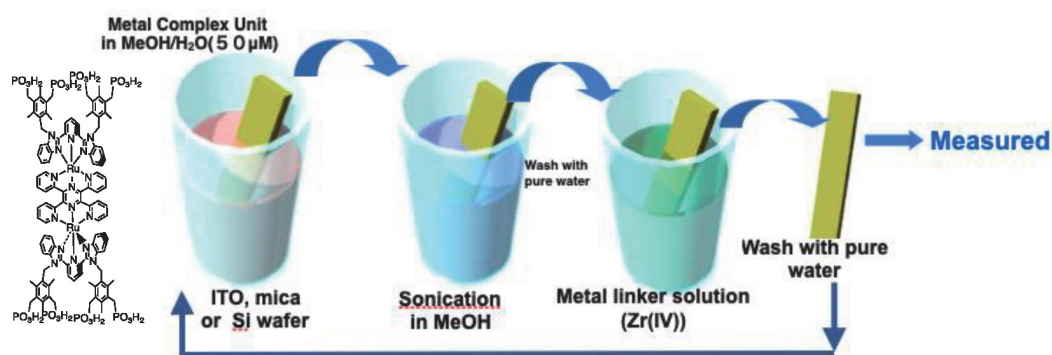


Figure 17. Illustration of the layer-by-layer (LbL) assembly by successive immersion of a solid substrate such as ITO, mica, or a Si wafer into (i) a solution of a given Ru complex with phosphonate anchors, and (ii) a solution of Zr(IV) ions. After washing, this immersion process was conducted repeated several times.

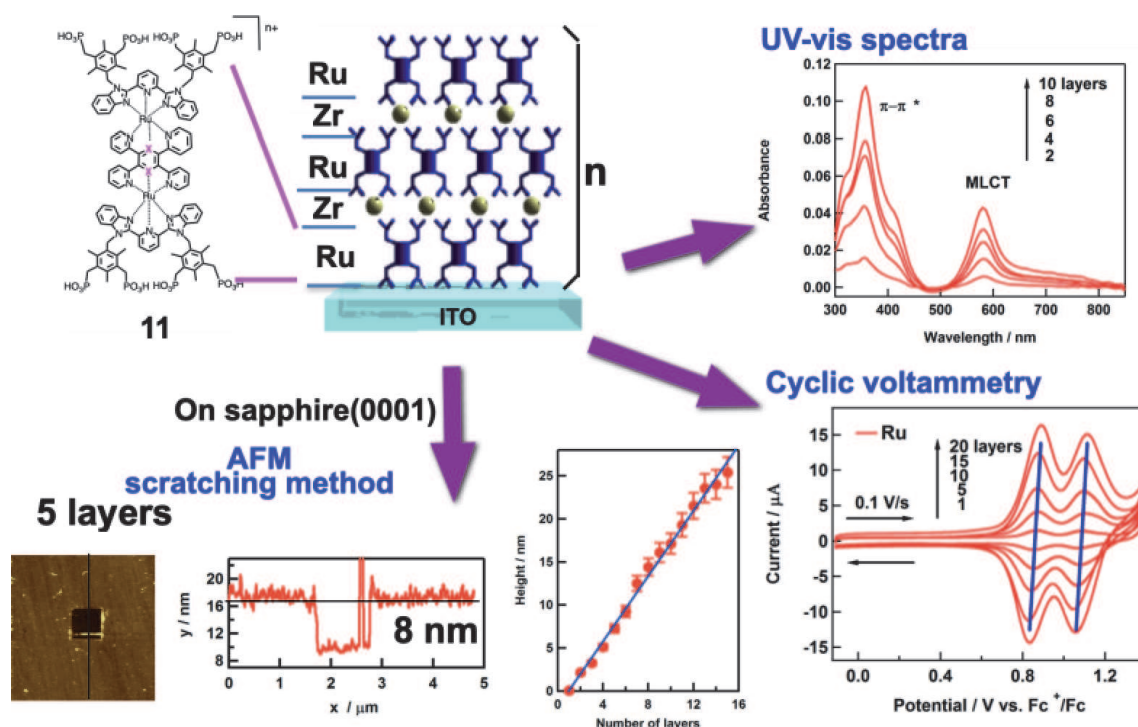


Figure 18. Illustration of the LbL multilayer film of **11** and monitoring of its LbL growth using UV-vis spectroscopy, CV, and the AFM-scratching method, together with a plot of the height of the scratch vs. the number of layers.

the linear increase in the physical quantities such as absorbance indicates the formation of well-ordered two-dimensional multilayer films on the solid surfaces.

The use of the LbL method on a solid surface makes it possible to accumulate various molecular units with different chemical functionalities by adjusting the number of layers and metals in the multilayer films. Furthermore, the sequential order of the various complex units can be varied; the units can be arranged in order of descending or ascending potential or pK_a to produce hetero-multilayer films. Such gradients in the layers play an important role in energy transduction. Therefore, “coordination programming” at the surface is possible via judicious choice of molecular units [60]. For example, when two different complexes A and B are assembled into a four-layered film on a solid substrate and a primer layer A is fixed as the first immobilized layer, seven combinations can be obtained by varying the order of the successive layers (substrate|ABAB, |AAAB, etc.). As a result, various films with different potential gradients can be created, and their rectification of electron transfer can be evaluated. Finally, in the fabrication of heterolayers using

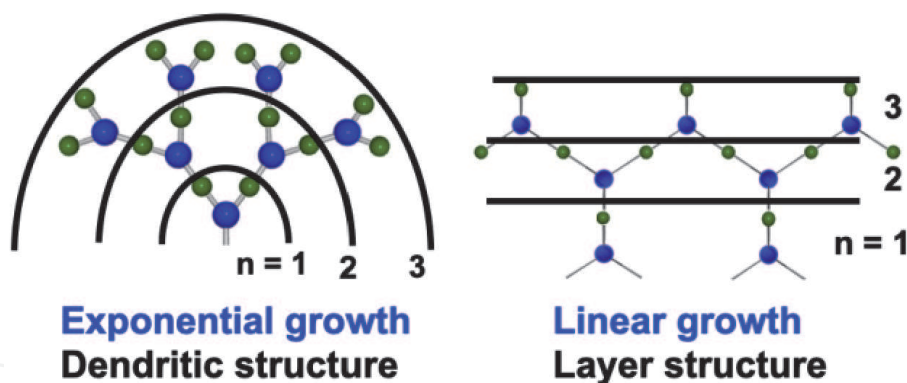


Figure 19.

Illustration of two-layer-growth models: Dendritic divergent growth (left) and linear growth (right) [58].

metal-coordination via the LbL method by immersion in solutions of each component, it is important to ensure that each layer is segregated and that the components are not mixed with others within the layer. In particular, care should be taken using metal ions with substitutionally labile properties, such as Ni(II) and Co(II) ions.

3.4 Functionality of LbL-multilayer films based on Ru complexes

3.4.1 Electron-transfer rate in homo-multilayer Ru complex films on ITO electrodes

Measuring electron-transfer events in multilayer LbL films composed of redox-active Ru complexes on an ITO electrode is fundamental to determine whether electrons can be transmitted through the multiple layers of Ru complexes as the number of layers is increased.

CV measurements of homo-multilayer films of **11** ($X = N$) to evaluate their electron-transfer rate showed two one-electron oxidation waves. With increasing number of layers, the peak current during CV increased almost linearly. The peak-potential separation between the anodic and cathodic waves was unchanged at a scan rate of $0.1 \text{ V}\cdot\text{s}^{-1}$, but at $1 \text{ V}\cdot\text{s}^{-1}$, the separation increased with an increasing number of layers. Using Laviron's procedure, [61] the heterogeneous electron-transfer rate between the Ru complexes in the layers and the ITO electrode was determined for different numbers of layers. The electron-transfer rates gradually decreased with increasing number of layers, and a small attenuation coefficient was obtained from the slope of the plots of $\ln(k_{\text{app}})$ as a function of the thickness of films (L). The dependence of the electron-transfer rate, k_{app} , on the distance is expressed by the following equation:

$$k_{\text{app}} = k^0 \exp \{-\beta L\} \quad (4)$$

In addition, potential-step chronoamperometry (PSCA) measurements furnished a relatively small value for the apparent electron-transfer rate, k_{app} ($\beta = 0.014 \text{ \AA}^{-1}$) [62].

Multi-layer films of ruthenium complex **9** were grown on an ITO substrate using hydrogen-bonding interactions. In these films, free-standing ruthenium complexes of **9** adsorbed on an ITO electrode via its tetrapod phosphonic acid anchors interacts with complexes of **9** that are dissolved in the solution via multiple hydrogen bonds between the free phosphonic acid groups at its surface and those of the complex **9** in solution at pH = 6. Surprisingly, the film thickness of the resulting multiply hydrogen-bonded system was controlled by the immersion time and the solution

pH. The current–voltage (I – V) characteristics of the multilayered Ru film grown on ITO were measured with a sandwich-type two-terminal devices using the conductive polymer PEDOT:PSS as the top electrode. Based on the observed current, the value of the coefficient for the attenuation with increasing film thickness was relatively small ($\beta = 0.012$ – 0.021 \AA^{-1}) [43]. This small β value for the multilayer Ru complex film system indicates that long-range electron transport can be expected to be possible even though the system exhibits low conductivity. To clarify the reason for the long-range electron transport in the Ru multilayer film despite its low conductivity, first-principles calculations using Green’s non-equilibrium function technique and theoretical analysis of the experimental results were performed. The results indicated that the metal centers covered with the π electrons of the ligands become “stepping stone” sites that provide a resonant tunneling mechanism [43]. Small β values were also reported for terpyridine-metal-complex nanowires produced by the sequential metal-coordination method [63].

3.4.2 Redox-active LbL multilayer films in redox capacitors

As portable electronic devices continue to proliferate, cost-effective cheap energy storage devices that are small, flexible, and low cost and provide high performance during the charging and discharging cycle are in high demand. Molecular-based supercapacitors are promising candidates in terms of these requirements. Redox-active Ru complexes are suitable for the fabrication of energy storage devices, since multilayer molecular Ru assemblies obtained via the LbL method can be scaled by increasing the number of layers, which leads to enhancement of the electrical capacitance in such films [57].

The charge–discharge properties of a sixty-five-layer film of Ru complex **11**, ITO|(Ru complex **11**)₆₅, were examined under galvanostatic experimental conditions by applying various constant current densities from 10 to 100 $\mu\text{A}\cdot\text{cm}^{-2}$. The galvanostatic charge and discharge curves show two small plateaus at 0.12 V and 0.37 V vs. Pt, which correspond to two reversible Ru(II)/Ru(III) redox processes (**Figure 20**). A maximum capacitance of $92.2 \text{ F}\cdot\text{g}^{-1}$ was found at an applied current density of 10 $\mu\text{A}\cdot\text{cm}^{-2}$, but the capacitance decreased to $63.3 \text{ F}\cdot\text{g}^{-1}$ at the highest

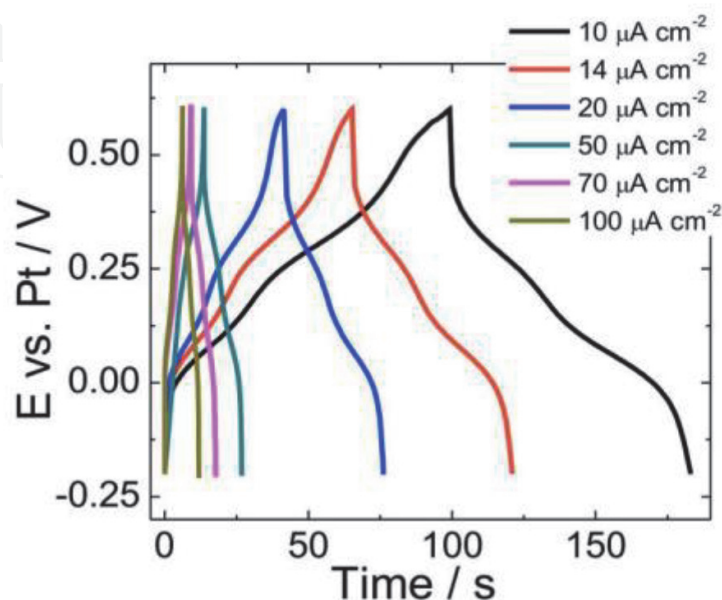


Figure 20.
 Galvanostatic charge–discharge curves of ITO|(Ru complex **11**)₆₅ in $\text{CH}_3\text{CN}/0.1 \text{ M HClO}_4$ at different current densities [57].

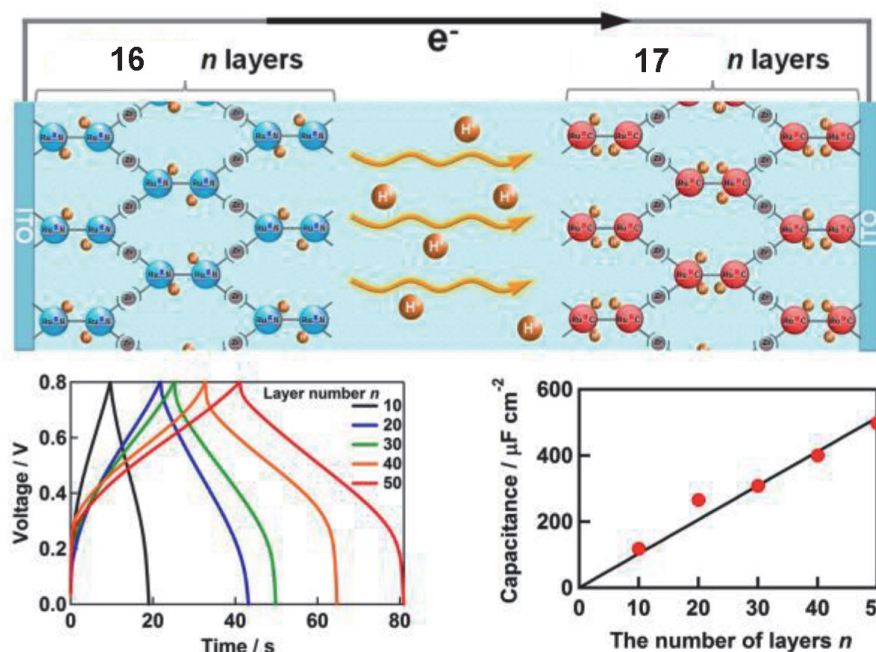


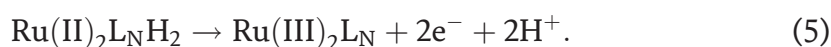
Figure 21. Schematic illustration of two half-cells composed of multilayer ITO/(**16**)_n and ITO/(**17**)_n (top), galvanostatic charge–discharge curves for **16** and **17** with different layer numbers, *n* (bottom left), and a plot of the capacitance as a function of *n* (bottom right) [20].

current density of $100 \mu\text{A}\cdot\text{cm}^{-2}$ (**Figure 20**). Stability tests of the Ru multilayer films (>1000 galvanostatic charge–discharge cycles) showed a capacitance retention of 72% [57].

3.4.3 PCET reactions in Ru-multilayer films for energy storage devices

PCET reactions can be used in energy-storage devices such as redox-flow batteries or two half-cells in unbuffered aqueous solution as described in Section 4.2. The frameworks of dinuclear Ru complexes **16** and **17** are basically formed by chemical modification of the mononuclear Ru complexes **13** and **14** via the C–C coupling of two **13** or **14** units. Thus, the PCET behaviors of complexes **16** and **17** were almost the same as those of **13** and **14**, except that the number of electrons involved in the PCET reaction was doubled to result in a two-electron process due to the C–C coupling of two molecular units of **13** and **14** and the surface immobilization on an electrode. The Ru complexes **16** and **17** were immobilized by the LbL method on an ITO electrode and applied in a redox capacitor device, in which an aqueous solution was sandwiched between two electrodes composed of multilayer films of **16** and **17** to evaluate the cell performance (**Figure 21**) [20]. Under galvanostatic conditions at a constant current density of $10 \mu\text{A}\cdot\text{cm}^{-2}$, stable charge–discharge behavior occurred, as shown in **Figure 21**.

During the charging process, the multilayer **16** acted as the anode and the following oxidation reaction proceeded, resulting in the release of protons:



At the same time, the multilayer electrode of **17** acted as a cathode, and the following reduction took place, resulting in the capture of protons:



where **16** and **17** are represented as $\text{Ru}_2\text{L}_\text{N}\text{H}_n$ and $\text{Ru}_2\text{L}_\text{C}\text{H}_n$, and $\text{L}_\text{N}\text{H}_n$ and $\text{L}_\text{C}\text{H}_n$ indicate the bridging ligand bearing the indicated number of protons on the benzimidazole groups. In other words, the capacitance increased with an increasing number of layers [20].

On the other hand, when all four imino N–H protons on the benzimidazole moieties were protected by N–Me groups, the capacitance decreased by 77% compared to that of the original PCET-type capacitor. This result strongly suggests that the proton movement plays a more important role than the anion movement in the charge storage. Furthermore, the proton movement accompanying the redox reaction in the Ru multilayer films on the ITO electrode was confirmed using a pH-indicator probe in aqueous solution. In this type of LbL films composed of Ru complexes that exhibit PCET-type redox reactions, the capacitance increases almost linearly with the number of layers (**Figure 21**) [20].

To obtain proton rocking-chair-type redox capacitors that use protons as the charge carriers, the quinone/hydroquinone couple is often used [52, 64–67]. However, at neutral pH, the electron–proton transfer rate of the quinone/hydroquinone couple is slower than that of the Ru(II/III) couple. The use of the LbL method to fabricate multilayered structures of redox-active Ru complexes that exhibit PCET is advantageous, as the storage capacity can be enhanced by increasing the number of redox-active modular units on demand.

3.5 Sequentially assembled heterolayer films of Ru complexes

One advantage of the LbL assembly method using metal coordination at the interface is that a combinatorial approach can be employed to construct sequentially ordered hetero-multilayer films (cf. Section 4.3).

Monolayer films of the Ru complexes **11** and **12** on ITO showed two well-defined CV waves at +0.83 and +1.04 V and at –0.37 and +0.09 V vs. Fc^+/Fc , which were assigned to Ru(II)–Ru(II)/Ru(II)–Ru(III) and Ru(II)–Ru(III)/Ru(III)–Ru(III) processes, respectively. Due to the large differences between the potentials of **11** and **12**, heterolayer films made from combinations of **11** and **12** exhibited interesting electronic/photonic behaviors such as electron-transfer blocking, rectification, and vectorial photoelectron transfer. **Figure 22** shows the CV responses of the heterolayer films $\text{ITO}|(\mathbf{11})_n/(\mathbf{12})_n$ ($n = 1, 2$, where n stands for the number of layers) and $\text{ITO}|(\mathbf{12})_n/(\mathbf{11})_n$ ($n = 1, 3$) and the alternating heterolayer films $\text{ITO}|(\mathbf{11}/\mathbf{12})_4$ and $\text{ITO}|(\mathbf{12}/\mathbf{11})_4$ in CH_3CN (0.1 M HClO_4) [22, 62]. The $\text{ITO}|(\mathbf{11})_1/(\mathbf{12})_1$ bilayer hetero-film exhibited four waves (**Figure 22a**), which correspond to the redox processes from both the inner **11** and outer **12** layers; the Ru(II)–Ru(III)/Ru(III)–Ru(III) process of **11** and the Ru(III)–Ru(III)/Ru(III)–Ru(IV) process of **12** overlap at +1.11 V. However, the peak separation of the outer layer of **12** increased at higher scan rates, while the peak separation for the waves from the inner layer of **11** remained unaffected. This result indicated a slower ET rate from the outer layer of **12** due to the higher spatial separation relative to the inner **11** film [22].

Conversely, for the $\text{ITO}|(\mathbf{11})_2/(\mathbf{12})_2$ hetero-film, in the first scan over the potential range of –0.5 V to +0.7 V vs. Fc^+/Fc , only oxidative waves from **11** at +0.83 and +1.04 V vs. Fc^+/Fc were present; no waves from the outer **12** layer were observed (see blue line in **Figure 22a**). However, when the potential was scanned in the negative direction to –0.5 V, a large cathodic wave appeared at approximately –0.5 V vs. Fc^+/Fc , and subsequently, a new anodic pre-peak at approximately +0.64 V (marked as x) was observed in the potential scan in the positive direction. The new pre-peak x was assigned as a catalytic oxidation wave derived from the ET of the outer **12** layers through ET mediation; that is, direct ET from the outer **12** layer to the electrode was blocked by the bilayer of **11**, and an avalanche ET from

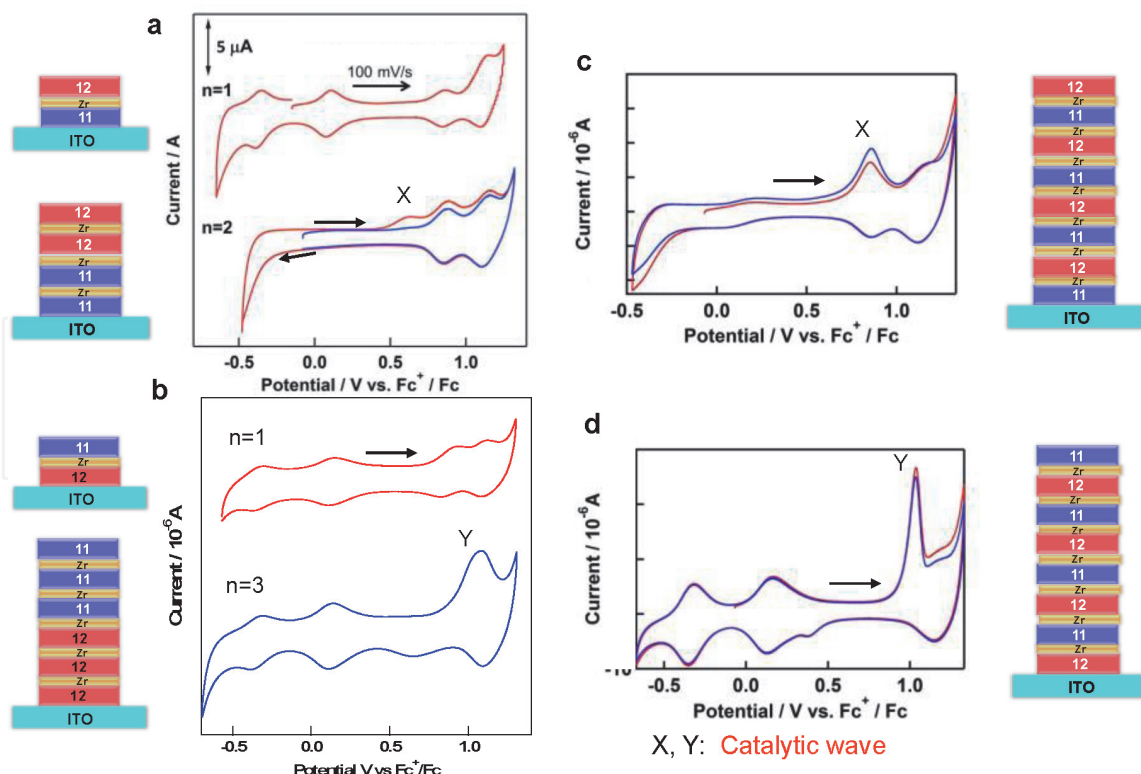


Figure 22.

Cyclic voltammograms of heterolayer films of Ru complexes **11** and **12** with varying sequences: (a) ITO/(**11**)_n/(**12**)_n (n = 1, 2, where n stands for the number of layers), (b) ITO/(**12**)_n/(**11**)_n (n = 1, 3), (c) alternating ITO/(**11/12**)₄ and (d) ITO/(**12/11**)₄ in CH_3CN (0.1 M HClO_4) [22, 62].

the outer **12** layers to the inner holes in **11** occurred through the potential gradient once a hole was generated in the inner **11** layers at the onset of the first **11** oxidation wave (Figure 23). Consequently, the large cathodic peak at -0.5 V was assigned to the catalytic reduction wave of the **12** film mediated by the reduction process of the inner **11** film. Furthermore, the sequence of the **11** and **12** layers on the ITO electrode leads to characteristic CV responses depending on the sequence and the number of layers, as shown in Figure 22 [62].

Silicon-based *pn* heterojunctions play an important role in various types of electronic devices, such as diodes, transistors, solar cells and light-emitting diodes (LEDs). The potential difference at the *pn* junction causes blockage of charge transport, resulting in a rectification effect. Under photoirradiation, current flows through the external circuit, which acts as a silicon-based solar cell. Similarly, the photo-response of Ru-complex heterolayer films has been examined [22]. Photoirradiation of the ITO/(**11**)₄/(**12**)₄ hetero-multilayer film in CH_3CN (0.1 M HClO_4) at the open circuit potential of +0.45 V produced a *cathodic photocurrent*. The action spectrum of this film is nearly identical to the UV-vis absorption

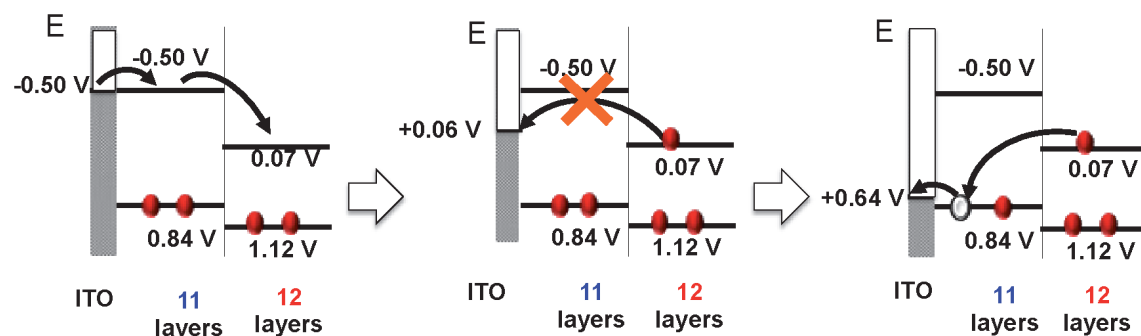


Figure 23.

Rectified ET mechanism for the CV response of the ITO/(**11**)₂/(**12**)₂ hetero-film shown in Figure 22a [22].

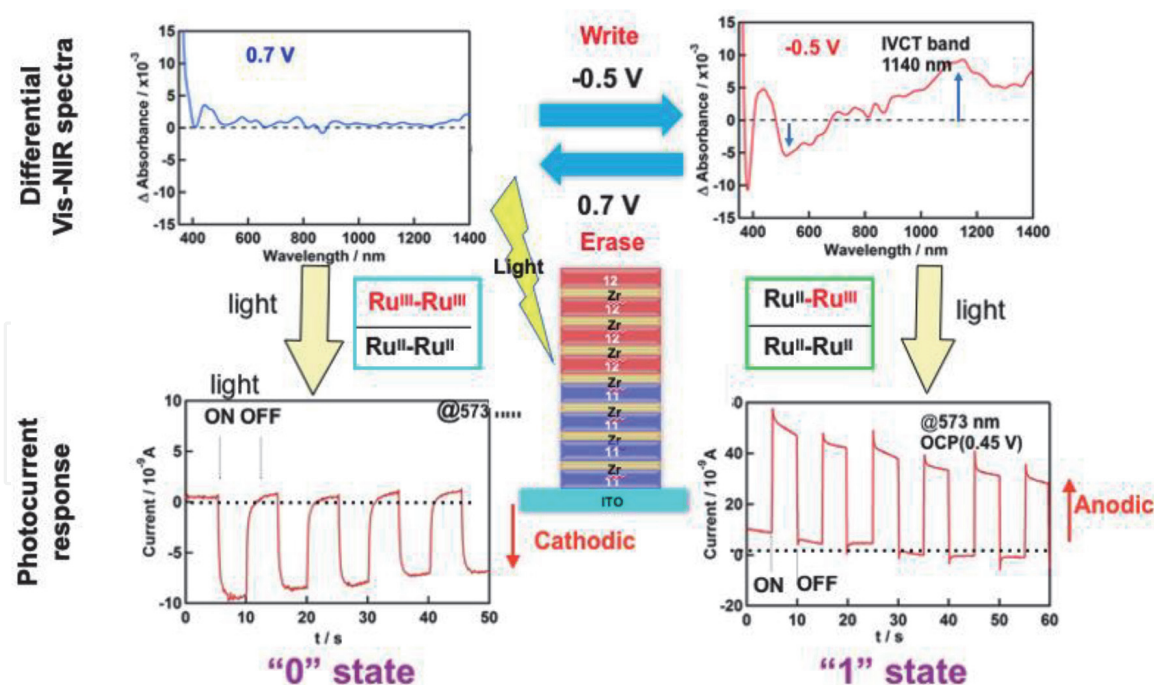


Figure 24. Switching between the “0” and “1” states by applying potentials of -0.5 V and $+0.7$ V in the ITO/(**11**)₄/(**12**)₄ hetero-film (top), and the corresponding photocurrent responses (bottom) [22].

spectrum of **11**, which indicates the inner **11** layers are the main contributor to the photoexcitation, although little photo-response was observed for homo-Ru-complex multilayer films such as ITO|(**11**)_n or ITO|(**12**)_n. Interestingly, the direction of the photocurrent on the ITO|(**11**)₄/(**12**)₄ heterolayer film switched from *cathodic* to *anodic* after the application of a potential pulse at -0.5 V. This photo-response change arose from the generation of a charge trapping state after the application of the pulse; the outer layers of **12** were reduced by the potential, and this reduced state was maintained as a charge-trapping state until holes were generated on the inner **11** layers by electrochemical oxidation or photoexcitation. This charge trapping state was recognized from the differential Vis-NIR spectra, in which a new inter-valence charge-transfer (IVCT) band at 1140 nm appeared for the mixed-valence state of **12** (**Figure 24**). Thus, the heterolayer film ITO|(**11**)₄/(**12**)₄ represents a typical example of a photo-responsive memory device; the writing process is achieved by applying a potential of either -0.5 or $+0.7$ V, and the readout process is achieved by measuring the direction of the photocurrent [22]. Accordingly, the judicious selection of both redox potentials and the sequential ordering of the Ru modular units on the ITO surface makes it possible to design functional electronic devices such as molecular diodes and memory devices.

4. Molecular-device applications using Ru complexes on ITO

The idea of molecular devices is based on a next-generation paradigm to overcome the limitations associated with Moore’s law, which states that the number of transistors per silicon chip doubles every year, and the use of individual molecules as active electronic components. The first single molecular device was the theoretical proposal of a molecular diode by Aviram and Ratner; [68] subsequently, the concept of molecular electronic devices was further developed by Carter [69]. Various molecules have demonstrated basic electronic functionality as switches, as diodes for rectification, and as optical devices, storage devices, and sensing devices

for future information technologies [54, 70]. The recent experimental development of single-molecular conductance measurements using metal–molecule–metal junctions [71] has opened a new avenue for the realization of molecular electronic devices through the judicious selection of molecules [70, 72–76]. Ru complexes are substitutionally inert in both the Ru(II) and Ru(III) oxidation states, and also exhibit fast self-exchange ET rates due to the small reorganization energy of the Ru (II/III) couple. Therefore, the use of a mixed-valence Ru(II)–Ru(III) complex as a perturbing motif branching from a conducting molecular wire has been proposed by Carter. Here, two molecular devices based on Ru complexes are discussed; the first is a Ru-complex molecular junction that exhibits rectification switching in response to humidity, and the other is a two-terminal memristor device based on the PCET reactions of Ru complexes.

4.1 Rectification switching in Ru complex molecular junctions in response to external humidity

Conductive-probe atomic force microscopy (C-AFM) was employed to measure the I – V characteristics of self-assembled monolayers of Ru complexes on an ITO electrode. An ITO-coated Pt probe was used as the C-AFM tip in order to employ the same material for the top and bottom electrode, and the I – V curves were measured via the two-terminal method [77].

Under dry (low humidity) conditions, the I – V plots of both mononuclear **10** and dinuclear complex **11** became symmetric in the positive and negative potential range, indicating that the molecules at the junction behaved as a molecular wire or resistor (Figure 25). However, under the wet (high humidity) conditions, the I – V curves became asymmetric and showed diode-like behavior *only* for dinuclear Ru complex **11**, while they remained symmetric for **10**. The rectification ratio R ($= |I(-V)|/|I(V)|$) was found to have a high value of ~ 1000 , where $|I(V)|$ represents the absolute value of the forward or reverse current density at a certain voltage. When the measurement conditions were changed from wet to dry, the I – V plots for **11** became symmetric again. This rectification switching via humidity change occurred repeatedly for **11** (Figure 26); conversely, such switching was not observed for **10** [77].

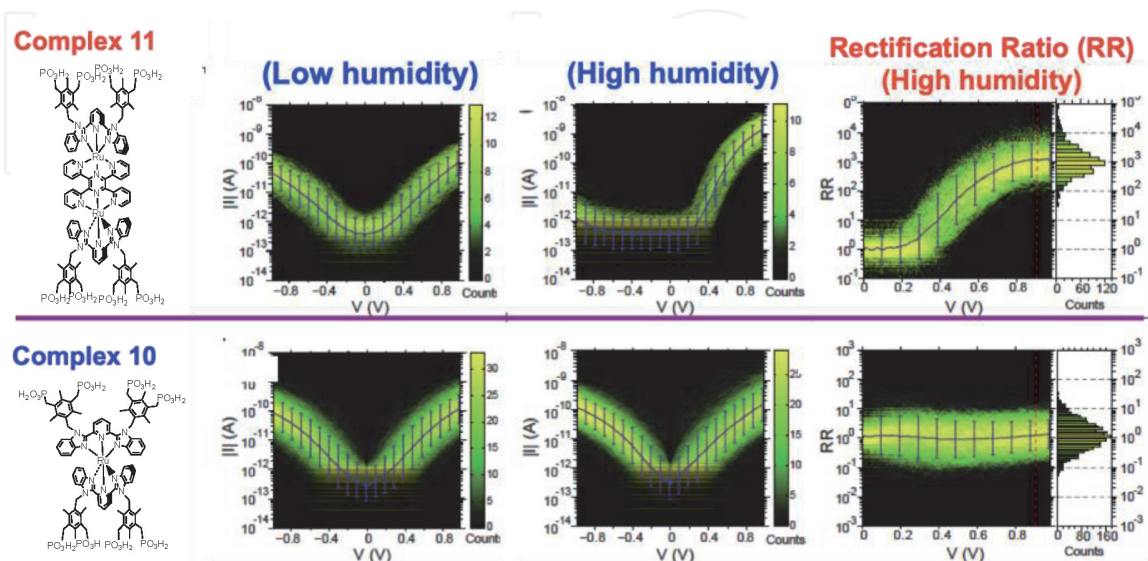


Figure 25.

Structures of Ru complexes **10** (top) and **11** (bottom), log $|I|$ – V curves of the **10** and **11** molecular junctions under low humidity (5%) and high humidity (60%) conditions, and 2D histograms of the rectification ratio (R) at high humidity [77].

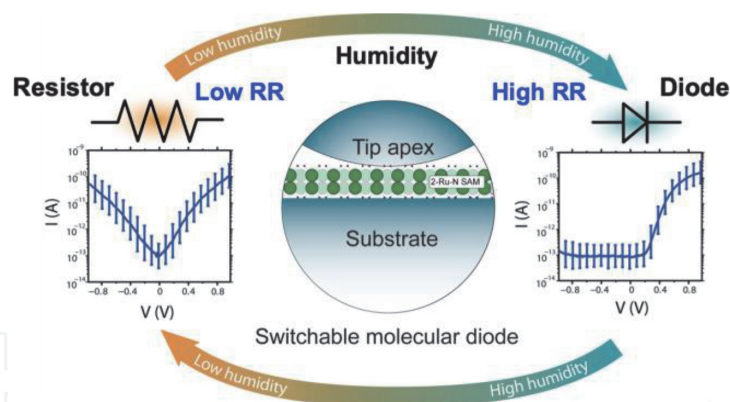


Figure 26.
 Conceptual illustration of a humidity-switchable molecular diode [78].

Several factors need to be considered to explain this behavior. The tip-radius affected the asymmetry of the I - V curves, whereby a small tip (50 nm radius) leading to a larger rectification ratio R on account that water molecules were more strongly attracted to the smaller tip. However, this effect could not fully explain the absence of asymmetry for **10**. Based on combined theoretical and experimental results, water molecules and counter-ion displacement have an important influence on two localized molecular orbitals in **11**, and under an applied voltage bias, a large asymmetry was induced externally via water molecules screening the counter-ions. Thus, via these rectifying properties, the self-assembled Ru complex **11** molecular junctions act as nanoscale sensors with ON/OFF switching in response to external humidity [77].

4.2 Protonic memristor devices based on Ru complexes with PCET

Recently, memristors have attracted substantial attention as the fourth passive element after resistors, capacitors, and inductors. The memristor was predicted by Chua in 1971 as a new electronic circuit element linking charge and magnetic flux, [79] and the first example of such a device was demonstrated experimentally in 2008. This first memristor device consisted of TiO_{2-x} sandwiched between two Pt metal terminals, in which the oxygen defects led to filament formation, and the defects acted as mobile charged dopants and drifted in the applied electric field [80]. As a result, the device exhibited a periodic pinched hysteresis loop in its I - V curves. Since then, not only metal oxides, but also many other materials such as organic polymers and metal chalcogenide films, have been sandwiched between the two terminals to fabricate devices with a non-linear hysteretic I - V loop [81, 82]. In the two-terminal devices, non-linear changes in the current occur during the voltage sweep, and the associated resistance changes. This type of electric element is generally referred to as a memristor. In recent years, the memristor has become relevant in the context of the action of synapses in the neuromorphic systems of the brain. In biological synapses, ion/molecule migration is used for signal transduction. Inspired by the ion migration in the synapse system, we developed a system in which a proton serves as the charge carrier at the interface between Ru complexes with PCET properties and a proton-conducting polymer such as poly(4-vinylpyridine) (P4VP). In Section 4.4.3, a charge-storage system was constructed from two electrodes modified with films of the Ru complexes **16** and **17**, which show PCET properties in unbuffered 0.1 M NaClO_4 solution, and the resulting two-terminal cells showed a stable charging-discharging process via a proton rocking-chair-type mechanism. The unbuffered aqueous solution was replaced with

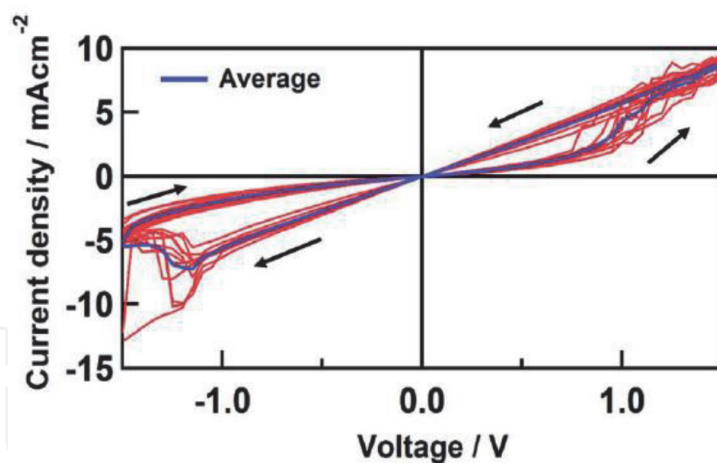


Figure 27.

I-V plots of the two-terminal device ITO/(16)₃/P4VP/(17)₃/ITO, showing ten scans on the same device. The blue line indicates the average of the ten scans [83].

proton-conducting P4VP ($pK_a \sim 4.0\text{--}5.2$), and the resulting two-terminal heterolayer device, ITO/(16)₃/P4VP/(17)₃/ITO, was tested. **Figure 27** shows the typical *I-V* characteristics of the two-terminal device, which produced “8” shaped and non-linear *I-V* loop curves [83].

To elucidate the coupling of the proton-transfer ability of P4VP and the PCET reactions of Ru complexes **16** and **17** at the hetero-interface, CV measurements were performed in 0.1 M NaClO₄ aqueous solution (**Figure 28**). A large negative potential shift was observed for the Ru(II/III) peak of the ITO/(16)₃/P4VP film compared to that of ITO/(16)₃ without P4VP. This negative potential shift arises from the hydrogen-bonding interactions between the N-H benzimidazolyl groups in **16** and the pyridine groups in P4VP, based on a previous study of the hydrogen-bonding interactions between the N-H imino groups in Ru-benzimidazole-derivative complexes and *N*-heteroaromatics such as pyridine [84]. In this study, the magnitude of the shift was strongly correlated to the pK_a values of both components (i.e., the complex and the heteroaromatic component) [84]. On the other hand, only a small potential shift was observed between the peak of the ITO/(17)₃/P4VP film and that of ITO/(17)₃ without P4VP. The difference between these two systems was attributed to the pK_a difference between the Ru complexes in the Ru(II) and Ru(III) oxidation states.

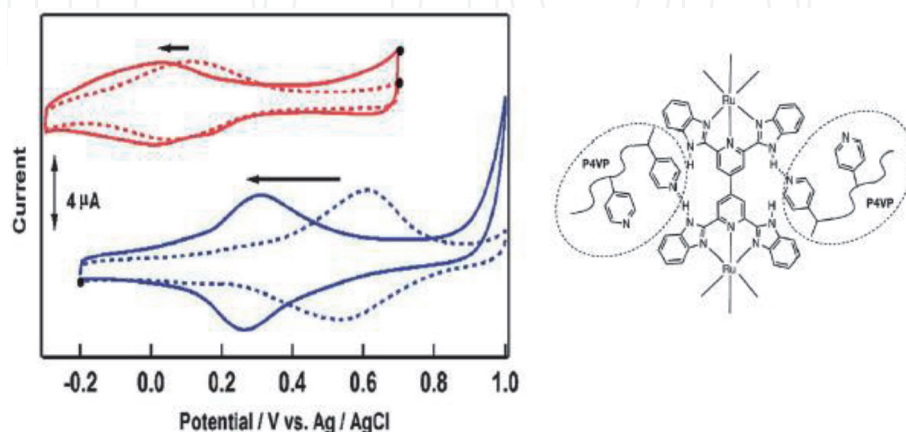


Figure 28.

*Cyclic voltammograms of ITO/(16)₃/P4VP (blue solid lines) and ITO/(17)₃/P4VP films (red solid lines), together with those of ITO/(16)₃ (blue dotted lines) and ITO/(17)₃ films (red dotted lines), in 0.1 M NaClO₄ aqueous solution, as well as a schematic illustration of the hydrogen-bonding interactions between the Ru complex **16** and the P4VP polymer [83].*

In the initial stage, the **16** site of the two terminal device ITO|(16)₃/P4VP/(17)₃|ITO is in the Ru(II) oxidation state with pK_a values in the range of 4.1–8.8, while the **17** site on the other side is in the Ru(III) state with pK_a values in the range of 5.2–9.8. The pK_a value of the intervening P4VP polymer is 4.0–5.2. Thus, the proton gradient across the interfaces is small, and it is equilibrated through hydrogen bonding between the P4VP and both **16** and **17** (Figure 29). When a bias potential of +1.5 V is applied to the two-terminal ITO|(16)₃/P4VP/(17)₃|ITO device, redox processes occur on the immobilized Ru complexes, namely, the oxidation of **16** from the Ru(II) state to Ru(III) takes place at the positive-potential side of the terminal, accompanied by the reduction of **17** from the Ru(III) state to Ru(II) at the other terminal. The resulting redox reactions induce large changes in the pK_a of **16** and **17** relative to those of their initial Ru(II) or Ru(III) states, resulting in a large proton gradient across the immobilized Ru complex/P4VP interfaces (Figure 11). Specifically, the pK_a of **16** drops to <3.8, which means that protons are easily released upon the oxidation of **16**, while on the **17** side, the pK_a increases to >8.4. Given the pK_a value of the intervening P4VP is 4.0–5.2, the (16)/P4VP proton transfer equilibrium is shifted toward the protonation of the P4VP side, while at the (17)/P4VP side, the equilibrium shifts toward the protonation of the film of **17** upon reduction of the Ru center. The proton conductivity through the protonated P4VP layer is improved by the resulting large pK_a gradient, resulting in enhanced conduction until the opposite redox reactions take place at both terminals. When the bias potential was scanned in the negative direction toward –1.5 V, the pK_a gradient returned to the initial state, and the current decreased in the absence of a driving force for electron or proton transport between **16**/P4VP and P4VP/**17**.

Therefore, the large pK_a difference in the Ru complexes **16** and **17** induced by the PCET redox reactions at the two terminals cause a proton gradient across the intervening proton-conducting P4VP, leading to high proton conductivity under an applied voltage. The change in the proton gradient due to the PCET redox reaction in the two-terminal device can be applied to use the proton-conducting switching devices as protonic memristors [83].

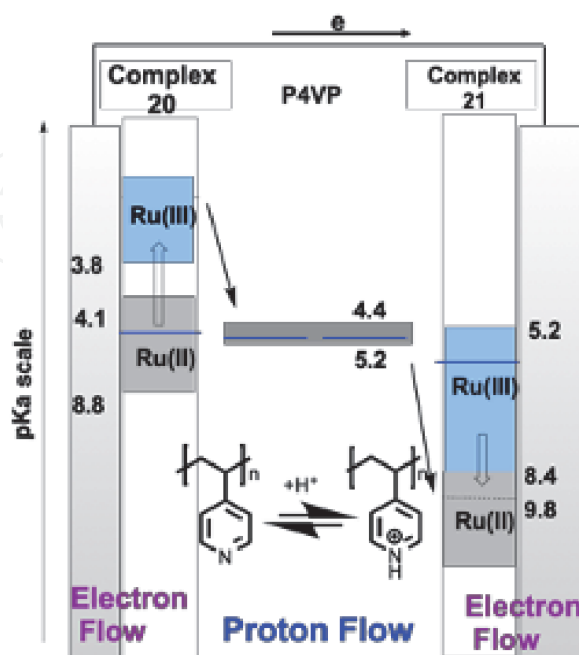


Figure 29. Schematic illustration of the proton-conduction switching in the two-terminal device ITO|(16)₃/P4VP/(17)₃|ITO and the pK_a gradient under the applied positive bias potential. The numbers refer to the pK_a values of the Ru(II) and Ru(III) complexes [83].

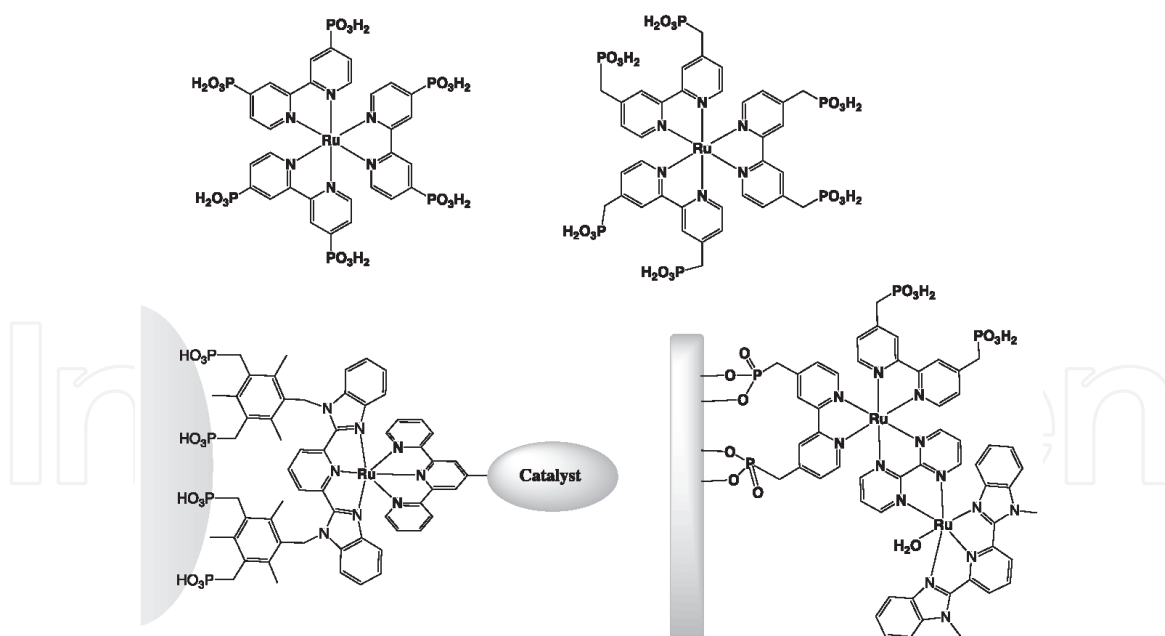


Figure 30.

Chemical structures of $\text{Ru}(\text{bpy})_3$ derivatives that contain phosphonic acid anchors and surface-confined Ru catalyst and chromophore-catalyst assemblies [85, 86].

5. Miscellaneous devices based on Ru–benzimidazole complexes for solar-energy transduction

Further important applications for ruthenium complexes include photoredox catalysts and dye-sensitized solar cells. In particular, $\text{Ru}(\text{bpy})_3$ or $\text{Ru}(\text{tpy})_2$ derivatives have been used as photosensitizer dyes on mesoporous TiO_2 surfaces in Grätzel-type solar cells. Over the past two decades, many Ru complexes with phosphonate anchors have been reported, [33] and many Ru dyes derived from $\text{Ru}(\text{bpy})_3$ derivatives that contain phosphonate anchors (**Figure 30**). Additionally, Ru-2,6-bis(benzimidazole-2-yl)pyridine complexes have been employed as photoredox catalysts [85, 86]. The Ru–benzimidazole bond is known to be more stable than the Ru–pyridine bond in the photoexcited state, rendering such Ru–benzimidazole complexes promising candidates for photoelectrochemical redox catalysts.

6. Conclusion

Substitutionally inert ruthenium complexes bearing benzimidazole derivatives have unique electrochemical and photochemical properties. In particular, proton-coupled electron-transfer in ruthenium–benzimidazole complexes endows them with rich redox chemistry and makes them useful as a modular unit for redox mediators or reactive sites for switching by external stimuli. In this chapter, the role of PCET reactions on Ru–benzimidazole complexes in energy-storage applications and the tuning of metal–metal interactions in aqueous solution was emphasized first. Based on this knowledge acquired from solution chemistry, the chemistry of Ru complexes confined on an electrode surface via their self-assembling from solution for the fabrication of the surface functional molecular devices on electrodes was discussed. Indium-tin oxide (ITO) is often chosen as the electrode due to its transparency and wide use as a substrate in electronics. To immobilize the redox-active Ru complexes on an ITO electrode, tetrapod phosphonic acid anchor groups

are often incorporated into tridentate 2,6-bis(benzimidazole-2-yl)pyridine or benzene ligands, which enables the construction of free-standing self-assembled monolayer structures on an ITO electrode. Starting from this monolayer as a primer layer, multilayer films can be constructed by the LbL layer growth method. The resulting multilayers using redox-active Ru complexes as a modular unit exhibited long-range electron transport even in films with over 60 layers (~100 nm thick) through the “stepping-stone” mechanism. Furthermore, a combinatorial approach to LbL layer growth can be used to obtain bespoke functional heterolayer films via material design. Using this strategy, blocking of electron transfer or rectification can be made to occur in such Ru complex heterolayer films, which results in charge trapping; the trapped electrons can subsequently be released via photo-irradiation, which leads to the new concept of photo-responsive memory devices. The CV response of multilayer films of Ru complexes with PCET depends strongly on the pH value. By judicious selection of the redox potentials and pK_a values of the two Ru complexes with PCET properties, two-electrode cells based on the Ru complex multilayer films that acted as proton rocking-chair-type redox capacitors can be obtained. Furthermore, by sandwiching a proton-conducting polymer between two Ru multilayer terminals, new type of protonic memristor device can be fabricated.

Therefore, surface-confined Ru complexes exhibit highly promising potential for the development of new functional molecular-based devices.

Acknowledgements

The author gratefully acknowledges financial support from MEXT via Grants-in-Aid for Scientific Research, No. 21108003 (Coordination Programming) and JP17H05383 (Coordination Asymmetry) as well as from the Institute of Science and Engineering at Chuo University. The author would also like to thank Dr. Katsuaki Kobayashi, Prof. Katsuhiko Kanaizuka, Dr. Hiroaki Ozawa, as well as all of his past students and coauthors in my papers for their great help and their contributions.

Dedication


This chapter is dedicated to my good friend Prof. Wolfgang Kaim on the occasion of his 70th birthday, and to my late wife, Masako Haga, who has supported my research activities for many years.

Author details

Masa-aki Haga
Research and Development Initiative, Chuo University, Tokyo, Japan

*Address all correspondence to: mhaga@kc.chuo-u.ac.jp

IntechOpen

© 2021 The Author(s). Licensee IntechOpen. This chapter is distributed under the terms of the Creative Commons Attribution License (<http://creativecommons.org/licenses/by/3.0>), which permits unrestricted use, distribution, and reproduction in any medium, provided the original work is properly cited. 

References

- [1] Higgins S. Regarding ruthenium. *Nat Chem.* 2010;2:1100-1100.
- [2] Seddon EA, Seddon KR. *The Chemistry of Ruthenium.* Amsterdam, The Netherlands: Elsevier; 1984.
- [3] Holder AA, Lilge L, Browne WR, Lawrence MAW, Bullock JL, editors. *Ruthenium Complexes: Photochemical and Biomedical Applications.* Weinheim, Germany: Wiley-VCH; 2018.
- [4] Juris A, Balzani V, Barigelli F, Campagna S, Belser P, von Zelewsky A. Ru(II) Polypyridine Complexes: Photophysics, Photochemistry, Electrochemistry, and Chemiluminescence. *Coord. Chem. Rev.* 1988, 84:85-277.
- [5] Campagna S, Puntoriero F, Nastasi F, Bergamini G, Balzani V. Photochemistry and Photophysics of Coordination Compounds: Ruthenium. *Top. Curr. Chem.* 2007; 280: 117 – 214.
- [6] Ceroni P, Bergamini G, Balzani, V. Old Molecules, New Concept: [Ru(bpy)₃]²⁺ as a Molecular Encoder-Decoder. *Angew. Chem. Int. Ed.* 2009; 48(45):8516-8518.
- [7] Burstall FH. Optical Activity dependent on Co-ordinated Bivalent Ruthenium. 34. Optical activity dependent on co-ordinated bivalent ruthenium. *J Chem Soc.* 1936:173 - 175.
- [8] Kalyanasundaram K. *Photochemistry of polypyridine and porphyrin complexes.* London, San Diego: Academic Press; 1992.
- [9] Haga M, Tanaka T. Synthesis and properties of mixed-ligand ruthenium (ii) complexes containing 2-(2-pyridyl) benzimidazole and related ligands. *Chem Lett.* 1979;8(7):863-864.
- [10] Haga M. Synthesis and protonation-deprotonation reactions of ruthenium (ii) complexes containing 2,2'-bibenzimidazole and related ligands. *Inorg Chim Acta.* 1983;75:29 - 35.
- [11] Liu Q, Zhao X, Hu Z, Zhao Z, Wang H. Synthesis and structural studies of N-heterocyclic carbene Ag(I) and Hg(II) complexes and recognition of dihydrogen phosphate anion. *Sci Rep.* 2017;7(1):7534. DOI: 10.1038/s41598-017-07961-8.
- [12] Roland S, Ling X, Pileni MP. N-Heterocyclic carbene ligands for Au nanocrystal stabilization and three-dimensional self-assembly. *Langmuir.* 2016;32(31):7683-7696. DOI: 10.1021/acs.langmuir.6b01458.
- [13] Haga M. Synthesis and properties of tris(2,2'-bibenzimidazole)ruthenium (II) dication, [Ru(BiBzImH₂)₃]²⁺. *Inorg Chim Acta.* 1983;77:L39-L41.
- [14] Xiaoming X, Haga M, Matsumura-Inoue T, Ru Y, Addison AW. Synthesis and proton transfer linked redox tuning of ruthenium(II) complexes with tridentate 2,6-bis(benzimidazol-2'-yl)pyridine ligands. *J Chem Soc Dalton Trans.* 1993:2477-2484.
- [15] Bond AM, Haga M. Spectrophotometric and voltammetric characterization of complexes of bis-(2,2'-bipyridine)(2,2'-bibenzimidazole) ruthenium and osmium in oxidation state II, III, and IV in acetonitrile-water mixtures. *Inorg Chem.* 1986;25:4507 - 4514.
- [16] Haga M, Ano T, Kano K, Yamabe S. Proton-induced switching of metal-metal interaction in dinuclear ruthenium and osmium complexes bridged by bis-2,2'-(2-pyridyl)-bibenzimidazole'. *Inorg Chem.* 1991;30: 3843 - 3849.

- [17] Haga M, Ali MM, Koseki S, Fujimoto K, Yoshimura A, Nozaki K, et al. Proton-induced tuning of electrochemical and photophysical properties in mononuclear and dinuclear ruthenium complexes containing 2,2'-bis(benzimidazol-2-yl)-4,4'-bipyridine: Synthesis, molecular structure, and mixed-valence state and excited-state properties. *Inorg Chem.* 1996;35(11):3335-3347. DOI: 10.1021/ic950083y.
- [18] Haga M, Hong H, Shiozawa Y, Kawata Y, Monjushiro H, Fukuo T, et al. Synthesis and proton-coupled electron transfer reaction of self-assembled monolayers of ruthenium(II) complex containing tridentate 2,6-bis(benzimidazol-2-yl)-pyridine on gold surface. *Inorg Chem.* 2000;39:4566 - 4573.
- [19] Kohmoto M, Ozawa H, Yang L, Hagio T, Matsunaga M, Haga M. Controlling the adsorption of ruthenium complexes on carbon surfaces through noncovalent bonding with pyrene anchors: An electrochemical study. *Langmuir.* 2016;32(17):4141-4152. DOI: 10.1021/acs.langmuir.6b00405.
- [20] Yoshikawa K, Motoyama D, Hiruma Y, Ozawa H, Nagano S, Haga M. Proton-rocking-chair-type redox capacitors based on indium tin oxide electrodes with multilayer films containing Ru complexes. *ACS Appl Mater Interfaces.* 2018;10(32):26990-27000. DOI: 10.1021/acsami.8b05907.
- [21] Haga M, Kobayashi K, Terada K. Fabrication and functions of surface nanomaterials based on multilayered or nanoarrayed assembly of metal complexes. *Coord Chem Rev.* 2007;251:2688-2701.
- [22] Nagashima T, Ozawa H, Suzuki T, Nakabayashi T, Kanaizuka K, Haga M. Photoresponsive molecular memory films composed of sequentially assembled heterolayers containing ruthenium complexes. *Chem – Eur J.* 2016;22:1658– 1667.
- [23] Haga M. Benzimidazole Ligands. In: McCleverty JA, Meyer TJ, editors. *Comprehensive Coordination Chemistry II, Vol. 1.* Elsevier Pergamon Press; Oxford, UK; San Diego, CA, USA, 2003. p. 125-134.
- [24] Haga M, Takasugi T, Tomie A, Ishizuya M, Yamada T, Hossain MD, et al. Molecular design of a proton-induced molecular switch based on rod-shaped Ru dinuclear complexes with bis-tridentate 2,6-bis(benzimidazol-2-yl)pyridine derivatives. *Dalton Trans.* 2003 (10):2069-2079. DOI: 10.1039/b300130j.
- [25] Haga M, Ano T, Ishizaki T, Kano K, Nozaki K, Ohno T. Synthesis and proton-coupled redox properties of mononuclear or asymmetric dinuclear complexes of ruthenium, rhodium, and/or osmium containing 2,2'-bis-(2-pyridyl)-bibenzimidazole. *J Chem Soc Dalton Trans.* 1994:263 - 272.
- [26] Ohno T, Nozaki K, Haga M. Metal-to-ligand charge transfer excited state of a biruthenium(II) compound bridged by 2,6-(2-pyridyl)benzodimidazole. *Inorg Chem.* 1992;31:4256 - 4261.
- [27] Yin J, Elsenbaumer RL. Efficient synthesis and characterization of novel bibenzimidazole oligomers and polymers as potential conjugated chelating ligands. *J Org Chem.* 2005;70: 9436 - 9446.
- [28] Yin J, Elsenbaumer RL. Syntheses of homochiral multinuclear Ru complexes based on oligomeric bibenzimidazoles. *Inorg Chem.* 2007;46:6891- 6901.
- [29] Galoppini E. Linkers for anchoring sensitizers to semiconductor nanoparticles. *Coord Chem Rev.* 2004; 248(13-14):1283-1297. DOI: 10.1016/j.ccr.2004.03.016.

- [30] Pujari SP, Scheres L, Marcelis ATM, Zuillhof H. Covalent surface modification of oxide surfaces. *Angew Chem Int Ed*. 2014;53(25):6322-6356. DOI: 10.1002/anie.201306709.
- [31] Cao Jr. R, Díaz-García AM, Cao R. Coordination compounds built on metal surfaces. *Coord Chem Rev*. 2009;253(9-10):1262-1275. DOI: 10.1016/j.ccr.2008.08.010.
- [32] Queffélec C, Petit M, Janvier P, Knight DA, Bujoli B. Surface modification using phosphonic acids and esters. *Chem Rev*. 2012;112(7):3777-3807. DOI: 10.1021/cr2004212.
- [33] Paniagua SA, Giordano AJ, Smith OL, Barlow S, Li H, Armstrong NR, et al. Phosphonic acids for interfacial engineering of transparent conductive oxides. *Chem Rev*. 2016;116(12):7117-7158. DOI: 10.1021/acs.chemrev.6b00061.
- [34] Materna KL, Crabtree RH, Brudvig GW. Anchoring groups for photocatalytic water oxidation on metal oxide surfaces. *Chem Soc Rev*. 2017;46(20):6099-6110. DOI: 10.1039/c7cs00314e.
- [35] Grätzel G. Mesoscopic solar cells for electricity and hydrogen production from sunlight. *Chem Lett*. 2005;34:8-13.
- [36] Bae E, Choi W, Park J, Shin HS, Kim SB, Lee JS. Effects of surface anchoring groups (carboxylate vs phosphonate) in ruthenium-complex-sensitized TiO₂ on visible light reactivity in aqueous suspensions. *J Phys Chem B*. 2004;108:14093-14101.
- [37] Zhang L, Cole JM. Anchoring groups for dye-sensitized solar cells. *ACS Appl Mater Interfaces*. 2015;7(6):3427-3455. DOI: 10.1021/am507334m.
- [38] Sakamoto K, Kuwae H, Kobayashi N, Nobori A, Shoji S, Mizuno J. Highly flexible transparent electrodes based on mesh-patterned rigid indium tin oxide. *Sci Rep*. 2018;8(1):2825. DOI: 10.1038/s41598-018-20978-x.
- [39] Dalle KE, Warnan J, Leung JJ, Reuillard B, Karmel IS, Reisner E. Electro- and solar-driven fuel synthesis with first row transition metal complexes. *Chem Rev*. 2019;119(4):2752-2875. DOI: 10.1021/acs.chemrev.8b00392.
- [40] Mallouk TE, Kim H-N, Ollivier PJ, Keller SW, editors. *Ultrathin Films Based on Layered Materials*. Oxford, UK: Pergamon; 1996.
- [41] Sevrain CM, Berchel M, Couthon H, Jaffrès PA. Phosphonic acid: preparation and applications. *Beilstein J Org Chem*. 2017;13:2186-2213. DOI: 10.3762/bjoc.13.219.
- [42] Haga M, Yutaka T. Inorganic supramolecular architectures at surfaces. In: Pombeiro AJL, Amatore C, editors. *Trends in Molecular Electrochemistry*: Marcel Dekker; 2004. p. 311-336.
- [43] Terada K, Nakamura H, Kanaizuka K, Haga M, Asai Y, Ishida T. Long-range electron transport of ruthenium-centered multilayer films via a stepping-stone mechanism. *ACS Nano*. 2012;6(3):1988-1999. DOI: 10.1021/nn300126m.
- [44] Loewe RS, Ambroise A, Muthukumaran K, Padmaja K, Lysenko AB, Mathur G, et al. Porphyrins bearing mono or tripodal benzylphosphonic acid tethers for attachment to oxide surfaces. *J Org Chem*. 2004;69:1453-1460.
- [45] Long B, Nikitin K, Fitzmaurice D. Self-assembly of a tripodal pseudorotaxane on the surface of a titanium dioxide nanoparticle. *J Am Chem Soc*. 2003;125:5152- 5160.
- [46] Kobayashi K, Tonegawa N, Fujii S, Hikida J, Nozoye H, Tsutsui K, et al. Fabrication of DNA nanowires by

orthogonal self-assembly and DNA intercalation on a Au patterned Si/SiO₂ surface. *Langmuir*. 2008;24:13203-13211.

[47] Gliboff M, Sang L, Knesting KM, Schalnatt MC, Mudalige A, Ratcliff EL, et al. Orientation of phenylphosphonic acid self-assembled monolayers on a transparent conductive oxide: A combined NEXAFS, PM-IRRAS, and DFT study. *Langmuir* 2013;29:2166-2174.

[48] Yang L, Ozawa H, Koumoto M, Yoshikawa K, Matsunaga M, Haga M. "Janus-type" ruthenium complex bearing both phosphonic acids and pyrene groups for functionalization of ITO and HOPG surfaces. *Chem Lett*. 2015;44(2):160-162. DOI: 10.1246/cl.140979.

[49] Kojima T. Development of functionality of metal complexes based on proton-coupled electron transfer. *Dalton Trans*. 2020;49(22):7284-7293. DOI: 10.1039/d0dt00898b.

[50] Huynh MHV, Meyer, TJ. Proton-Coupled Electron Transfer. *Chem. Rev*. 2007;107(11):5004-5064. DOI: 10.1021/cr0500030.

[51] Motoyama D, Yoshikawa K, Ozawa H, Tadokoro M, Haga M. Energy-storage applications for a pH gradient between two benzimidazole-ligated ruthenium complexes that engage in proton-coupled electron-transfer reactions in solution. *Inorg Chem*. 2017; 56(11):6419-6428. DOI: 10.1021/acs.inorgchem.7b00518.

[52] Emanuelsson R, Sterby M, Strømme M, Sjödin M. An all-organic proton battery. *J Am Chem Soc*. 2017;139(13): 4828-4834. DOI: 10.1021/jacs.7b00159.

[53] Tsitovich PB, Kosswattaarachchi AM, Crawley MR, Tittiris TY, Cook TR, Morrow JR. An Fe^{III} azamacrocyclic complex as a pH-Tunable catholyte and

anolyte for redox-flow battery applications. *Chem – Eur J*. 2017;23(61): 15327 - 15331.

[54] Liu D, Miao Q. Recent progress in interface engineering of organic thin film transistors with self-assembled monolayers. *Mater Chem Front*. 2018;2 (1):11-21. DOI: 10.1039/c7qm00279c.

[55] Decher G. Layered nanoarchitectures via directed assembly of anionic and cationic molecules. In: *Comprehensive Supramolecular Chemistry*. Volume 9: Templating, Self-assembly, and Self-organization. Atwood JL, Davies JED, Macnicol D, Vogtle F, editors: Elsevier Science Ltd.; 1996. p. 507-528.

[56] Ariga K, Ji Q, Hill JP, Bando Y, Aono M. Forming nanomaterials as layered functional structures toward materials nanoarchitectonics. *NPG Asia Mater*. 2012;4(5):e17. DOI: 10.1038/am.2012.30.

[57] Kaliginedi V, Ozawa H, Kuzume A, Maharajan S, Pobelov IV, Kwon NH, et al. Layer-by-layer grown scalable redox-active ruthenium-based molecular multilayer thin films for electrochemical applications and beyond. *Nanoscale*. 2015;7(42):17685-17692. DOI: 10.1039/c5nr04087f.

[58] Choudhury J, Kaminker R, Motiei L, de Ruiter G, Morozov M, Lupo F, et al. Linear vs exponential formation of molecular-based assemblies. *J Am Chem Soc*. 2010;132:9295-9297.

[59] Shinomiya T, Ozawa H, Mutoh Y, Haga M. A redox-active porous coordination network film based on a Ru complex as a building block on an ITO electrode. *Dalton Trans*. 2013;42 (45):16166-16175. DOI: 10.1039/c3dt51484f.

[60] Nishihara H. Coordination programming: A new concept for the creation of multifunctional molecular

systems. *Chem Lett.* 2014;43(4):388-395. DOI: 10.1246/cl.140010.

[61] Laviron E. General expression of the linear potential sweep voltammogram in the case of diffusionless electrochemical systems. *J Electroanal Chem. Interfacial Electrochem.* 1979;101:19-28.

[62] Nagashima T, Suzuki T, Ozawa H, Nakabayashi T, Oyama M, Ishida T, et al. Electrochemical behavior of sequentially assembled homo and heterolayer molecular films based on dinuclear ruthenium complexes. *Electrochim Acta.* 2016;204:235-244.

[63] Karipidou Z, Branchi B, Sarpasan M, Knorr N, Rodin V, Friederich P, et al. Ultrarobust thin-film devices from self-assembled metal-terpyridine oligomers. *Adv Mater.* 2016;28(18):3473-3480. DOI: 10.1002/adma.201504847.

[64] Er S, Suh C, Marshak MP, Aspuru-Guzik A. Computational design of molecules for an all-quinone redox flow battery. *Chem Sci.* 2015;6(2):885-893. DOI: 10.1039/c4sc03030c.

[65] Tomai T, Mitani S, Komatsu D, Kawaguchi Y, Honma I. Metal-free aqueous redox capacitor via proton rocking-chair system in an organic-based couple. *Sci Rep.* 2014;4:3591. DOI: 10.1038/srep03591.

[66] Ji Y, Goulet MA, Pollack DA, Kwabi DG, Jin S, Porcellinis D, et al. A phosphonate-functionalized quinone redox flow battery at near-neutral pH with record capacity retention rate. *Adv. Energy Mater.* 2019;9(12) DOI: 10.1002/aenm.201900039.

[67] Wedege K, Dražević E, Konya D, Bentien A. Organic redox species in aqueous flow batteries: Redox potentials, chemical stability and solubility. *Sci Rep.* 2016;6:39101. DOI: 10.1038/srep39101.

[68] Aviram A, Ratner MA. Molecular rectifiers. *Chem Phys Lett.* 1974;29:277 - 283.

[69] Carter FL. The molecular device computer: point of departure for larger scale cellular automata. *Physica D.* 1984; 10:175-194.

[70] Jeong H, Kim D, Xiang D, Lee T. High-yield functional molecular electronic devices. *ACS Nano.* 2017;11(7):6511-6548. DOI: 10.1021/acsnano.7b02967.

[71] Xu B, Tao NJ. Measurement of single-molecule resistance by repeated formation of molecular junctions. *Science.* 2003;301:1221-1223.

[72] Schwarz F, Kastlunger G, Lissel F, Riel H, Venkatesan K, Berke H, et al. High-conductive organometallic molecular wires with delocalized electron systems strongly coupled to metal electrodes. *Nano Lett.* 2014;14(10):5932-5940. DOI: 10.1021/nl5029045.

[73] Aradhya SV, Venkataraman L. Single-molecule junctions beyond electronic transport. *Nat Nanotechnol.* 2013;8(6):399-410 DOI: 10.1038/nnano.2013.91.

[74] Meng F, Hervault Y-M, Shao Q, Hu B, Norel L, Rigaut S, et al. Orthogonally modulated molecular transport junctions for resettable electronic logic gates. *Nat. Commun.* 2014;5:3023.

[75] Milan DC, Vezzoli A, Planje IJ, Low PJ. Metal bis(acetylide) complex molecular wires: concepts and design strategies. *Dalton Trans.* 2018;47:14125 - 14138.

[76] Tanaka Y, Kato Y, Tada T, Fujii S, Kiguchi M, Akita M. "Doping" of polyyne with an organometallic fragment leads to highly conductive metallapolyyne molecular wire. *J Amer Chem Soc.* 2018;140:10080 - 10084.

- [77] Atesci H, Kaliginedi V, Celis Gil JA, Ozawa H, Thijssen JM, Broekmann P, et al. Humidity-controlled rectification switching in ruthenium-complex molecular junctions. *Nat Nanotechnol.* 2018;13(2):117-121. DOI: 10.1038/s41565-017-0016-8.
- [78] https://mom.dcb.unibe.ch/mom_pages/mom_2018-02.html.
- [79] Chua L. Memristor-The missing circuit element. *IEEE Trans Circuit Theory.* 1971;18:507-519.
- [80] Strukov DB, Snider GS, Stewart DR, Williams RS. The missing memristor found. *Nature* 2008;453(7191):80-83. DOI: 10.1038/nature06932.
- [81] Bessonov AA, Kirikova MN, Petukhov DI, Allen M, Ryhanen T, Bailey MJA. Layered memristive and memcapacitive switches for printable electronics. *Nat Mater.* 2015;14(2):199-204. DOI: 10.1038/nmat4135.
- [82] Chua L. Five non-volatile memristor enigmas solved. *Appl. Phys. A.* 2018; 124(8):563. DOI: 10.1007/s00339-018-1971-0.
- [83] Hiruma Y, Yoshikawa K, Haga M. Bio-inspired protonic memristor devices based on metal complexes with proton-coupled electron transfer. *Faraday Discuss.* 2019;213:99-113. DOI: 10.1039/c8fd00098k.
- [84] Haga M, Tsunemitsu A. The outer-sphere interactions in ruthenium and osmium complexes I. Spectrophotometric and voltammetric studies on the hydrogen bonding interactions of bis(2,2'-bipyridine)(2-(2'-pyridyl)benzimidazole)ruthenium (II) cation and its derivatives with aromatic nitrogen heterocycles. *Inorg Chim Acta.* 1989;164:137-142.
- [85] Tamaki Y, Ishitani O. Supramolecular photocatalysts constructed with a photosensitizer unit with two tridentate ligands for CO₂ reduction. *Faraday Discuss.* 2017;198: 319-335. DOI: 10.1039/c6fd00220j.
- [86] Ashford DL, Gish MK, Vannucci AK, Brennaman MK, Templeton JL, Papanikolas JM, et al. Molecular chromophore-catalyst assemblies for solar fuel applications. *Chem Rev.* 2015; 115(23):13006-13049. DOI: 10.1021/acs.chemrev.5b00229.